Journal of Computational Physics 229 (2010) 7102–7128

Contents lists available at ScienceDirect

Journal of Computational Physics

journal homepage: www.elsevier.com/locate/jcp

A new approach of a limiting process for multi-dimensional flows

Hyung-Min Kang [a,1], Kyu Hong Kim [b,*], Dong-Ho Lee [c,2]

[a] BK21 School for Creative Engineering Design of Next Generation Mechanical and Aerospace Systems, BD. 312-202, Seoul National University, San 56-1, Shinrim-Dong, Kwanak-Ku, Seoul 151-744, South Korea
[b] School of Mechanical and Aerospace Engineering and Institute of Advanced Aerospace Technology, BD. 302-628, Seoul National University, San 56-1, Shinrim-Dong, Kwanak-Ku, Seoul 151-744, South Korea
[c] School of Mechanical and Aerospace Engineering and Institute of Advanced Aerospace Technology, BD. 301-1302, Seoul National University, San 56-1, Shinrim-Dong, Kwanak-Ku, Seoul 151-744, South Korea

ARTICLE INFO

Article history:
Received 14 November 2009
Received in revised form 31 May 2010
Accepted 2 June 2010
Available online 8 June 2010

Keywords:
Enhanced Multi-dimensional Limiting Process (e-MLP)
Multi-dimensional discontinuity
Higher order spatial accuracy
Distinguishing step

ABSTRACT

An enhanced Multi-dimensional Limiting Process (e-MLP) is developed for the accurate and efficient computation of multi-dimensional flows based on the Multi-dimensional Limiting Process (MLP). The new limiting process includes a distinguishing step and an enhanced multi-dimensional limiting process. First, the distinguishing step, which is independent of high order interpolation and flux evaluation, is newly introduced. It performs a multi-dimensional search of a discontinuity. The entire computational domain is then divided into continuous, linear discontinuous and nonlinear discontinuous regions. Second, limiting functions are appropriately switched according to the type of each region; in a continuous region, there are no limiting processes and only higher order accurate interpolation is performed. In linear discontinuous and nonlinear discontinuous regions, TVD criterion and MLP limiter are respectively used to remove oscillation. Hence, e-MLP has a number of advantages, as it incorporates useful features of MLP limiter such as multi-dimensional monotonicity and straightforward extensionality to higher order interpolation. It is applicable to local extrema and prevents excessive damping in a linear discontinuous region through application of appropriate limiting criteria. It is efficient because a limiting function is applied only to a discontinuous region. In addition, it is robust against shock instability due to the strict distinction of the computational domain and the use of regional information in a flux scheme as well as a high order interpolation scheme. This new limiting process was applied to numerous test cases including one-dimensional shock/sine wave interaction problem, oblique stationary contact discontinuity, isentropic vortex flow, high speed flow in a blunt body, planar shock/density bubble interaction, shock wave/vortex interaction and, particularly, magnetohydrodynamic (MHD) cloud-shock interaction problems. Through these tests, it was verified that e-MLP substantially enhances the accuracy and efficiency with both continuous and discontinuous multi-dimensional flows.

1. Introduction

Recently, there has been strong demand in several research areas for accurate supersonic/hypersonic computations that account for various types of discontinuity. These demands oblige the formulation of accurate and robust computations with

* Corresponding author. Tel.: +82 2 880 9346; fax: +82 2 887 2662.
E-mail addresses: kangm@snu.ac.kr (H.-M. Kang), aerocfd1@snu.ac.kr (K.H. Kim), donghlee@snu.ac.kr (D.-H. Lee).
[1] Tel.: +82 2 880 7399; fax: +82 2 882 7927.
[2] Tel.: +82 2 880 7386; fax: +82 2 882 7927.

0021-9991/$ - see front matter © 2010 Elsevier Inc. All rights reserved.
doi:10.1016/j.jcp.2010.06.001

very large grids and small size of time steps. However, the current level of technology does not meet the requirements of the Computational Fluid Dynamics (CFD) field yet; in a complex problem with millions of grid points, a considerable amount of computational time is needed and, thus far, stability problems continue to arise due to discontinuities. Therefore, for a significant enhancement of the applicability of CFD, the spatial scheme is required to be accurate even when fewer grid points are used and to be robust for highly nonlinear phenomena such as shock discontinuities.

In order to reduce the number of grid points and enhance the accuracy of CFD, higher order spatial interpolation schemes have been a good remedy. However, high order computations that take into account shock waves always induce unnecessary numerical oscillations near a discontinuity. Moreover, higher order schemes are not easy to extend to multi-dimensional supersonic applications because there are many problems in terms of stability and convergence. Therefore, the development of an effective multi-dimensional higher order scheme that removes numerical oscillations has become important so that CFD computations can retain their stability and convergence properties.

In order to resolve these problems, many studies have been carried out for seeking to introduce schemes that remove oscillation. The notable results are Total Variation Diminishing (TVD) [1–3], Essentially Non-Oscillatory (ENO) [4] and Total Variation Bounded (TVB) [5]. The concept of TVD was proven to be extremely successful because it gives a highly feasible result in the event of a discontinuity. However, the conventional TVD criterion is somewhat unsatisfactory near extrema due to clipping phenomena. Other concepts that overcome this weak point are the ENO and TVB schemes, which basically yield higher order spatial accuracy and an essentially non-oscillatory profile near a shock. However, because all of these were developed based on mathematical analyses of the one-dimensional scalar convection equation, they inevitably result in undershoot and/or overshoot when solving a multi-dimensional problem, even though they avoid unphysical clipping at extrema. For a stable and monotonic calculation of a multi-dimensional discontinuity, it is important to develop an oscillation removal process based on multi-dimensional flow phenomena.

Although there is no perfect means of extending schemes that remove oscillation to nonlinear multi-dimensional problems, Multi-dimensional Limiting Process (MLP) [6,7] may be feasible for oscillation removal in multi-dimensional flow problems. MLP enforces a property distribution that lies within the maximum and minimum value of the neighboring cells around cell-interface in the case of a steady problem. It shows a monotonic and stable calculation of the shock wave in multi-dimensional problems. However, MLP damps out the flow and is unsuitable for local extrema in a continuous region, which decreases the accuracy of the solutions. For these problems, a distinguishing criterion which determines whether a computational region is discontinuous or not is introduced in MLP and MLP limiter is then applied only to a discontinuous region [8]. However, it is relatively diffusive in a linear discontinuous region. Besides, widely used flux schemes do not always perform well in a discontinuity even though they show good characteristics when applied to gas dynamics problems. For example, in magnetohydrodynamic (MHD) problems, there have been many attempts to solve flows using Roe-type linearized Riemann solvers or HLL-type approximated Riemann solvers with conventional limiting functions. However, these methods are insufficient for oscillation removal, even in one-dimensional cases [9,10]. It is necessary to introduce appropriate numerical dissipation in a problematic region.

For effective oscillation removal, a discontinuous region has to be thoroughly distinguished and the information about the region needs to be considered in a flux scheme as well as a high order interpolation scheme. Therefore, an oscillation removal process should have the following features:

1.1. Separation of discontinuity search routine from high order interpolation

Generally, a discontinuity search routine is included in a dimensionally split interpolation scheme. Thus, information pertaining to the discontinuity is limited. This situation becomes an obstacle to the effective removal of the oscillation in a multi-dimensional flow or a complex flow such as a magnetohydrodynamic flow. To provide detailed information about a discontinuity to high order interpolation and flux evaluation simultaneously, the discontinuity search routine needs to be separated from an interpolation scheme. It also has to perform a thorough and multi-dimensional search of the discontinuous region.

1.2. Consideration of real flow physics in discontinuity search routine

In real flow physics, the flow phenomena include the combinations of various types of waves, such as expansion fan, contact discontinuity and shock wave. In accordance with this categorization, flows are also divided into continuous, linear discontinuous and nonlinear discontinuous types. For better accuracy, oscillation removal schemes need to consider the characteristics of each type. In addition, the excessive damping of the flow distribution must be suppressed, especially in continuous and linear discontinuous regions.

The objective of the present paper is to provide a new approach that reflects the features mentioned above as much as possible. Consequently, a new approach involving a multi-dimensional higher order scheme based on the Multi-dimensional Limiting Process (MLP) is introduced. It is termed as the enhanced Multi-dimensional Limiting Process (e-MLP). In this approach, a distinguishing step that is independent of an interpolation scheme and a flux scheme is introduced and discontinuities are sought in a comprehensive manner. Through this step, the computational domain is divided into continuous,

linear discontinuous and nonlinear discontinuous regions. This regional information is given to not only a high order interpolation scheme but also a flux scheme. Appropriate limiting criteria are then applied to each region in a high order interpolation scheme. Also, additional numerical dissipation is added to nonlinear discontinuous regions in a flux scheme. These increase the accuracy of the solution and make the computation robust against shock instability. Moreover, the computational cost is reduced because a limiting function is applied only to a discontinuous region.

The present paper is organized as follows. After a brief description of the governing equations in Section 2, the key ideas and overall procedure of e-MLP are explained in detail in Section 3. The distinguishing process and the switch of the limiting functions are described in Sections 4 and 5, respectively. In Section 6, various test cases are presented to verify the advantages of the proposed method. Finally conclusions based on the numerical tests and analyses are drawn in Section 7.

2. Governing equations

In this paper, the objective is to develop a newly enhanced version of MLP (e-MLP) that is appropriate for multi-dimensional flows including MHD problems. As general governing equations, Euler equations are presented in conservation form, as shown in Eq. (1).

$$\begin{aligned}
&\frac{\partial \rho}{\partial t} + \nabla \cdot (\rho \mathbf{V}) = 0, \\
&\frac{\partial \rho \mathbf{V}}{\partial t} + \nabla \cdot (\mathbf{V}\rho\mathbf{V}) + \nabla p = 0, \\
&\frac{\partial \rho e}{\partial t} + \nabla \cdot (\mathbf{V}\rho e + \mathbf{V}p) = 0,
\end{aligned} \tag{1}$$

where $\mathbf{V}$ is the velocity vector (u, v) and the equation of state of calorically perfect gas is given by

$$p = (\gamma - 1)\rho e = (\gamma - 1)\left(\rho e_t - \frac{1}{2}\rho \mathbf{V}^2\right), \quad \text{with } \gamma = 1.4 \text{ for air.} \tag{2}$$

For the ideal MHD formulation, the governing equations are written as Eq. (3).

$$\begin{aligned}
&\frac{\partial \rho}{\partial t} + \nabla \cdot (\rho \mathbf{V}) = 0, \\
&\frac{\partial \rho \mathbf{V}}{\partial t} + \nabla \cdot (\mathbf{V}\rho\mathbf{V} - \mathbf{B}\mathbf{B}) + \nabla p_{tot} = 0, \\
&\frac{\partial e}{\partial t} + \nabla \cdot (\mathbf{V}e + \mathbf{V}p_{tot} - \mathbf{B}\mathbf{B} \cdot \mathbf{V}) = 0, \\
&\frac{\partial \mathbf{B}}{\partial t} + \nabla \cdot (\mathbf{V}\mathbf{B} - \mathbf{B}\mathbf{V}) = 0,
\end{aligned} \tag{3}$$

where $\mathbf{B}$ is the magnetic field. Additionally, the sum of thermal and magnetic pressures is $p_{tot} = p + \mathbf{B}^2/2$ and the equation of state is presented as Eq. (4).

$$p = (\gamma - 1)\rho e = (\gamma - 1)\left(\rho e_t - \frac{1}{2}\rho \mathbf{V}^2 - \frac{1}{2}\mathbf{B}^2\right). \tag{4}$$

3. Key ideas of the enhanced Multi-dimensional Limiting Process

The key ideas of e-MLP can be summarized into three points. First, an independent distinguishing step, which is separated from high order interpolation and flux schemes, is introduced to a solver. Then, the computational domain is divided into continuous, linear discontinuous and nonlinear discontinuous regions. Second, based on the regional information, appropriate limiting functions are associated with each region in high order interpolation; in a continuous region, there is no limiting process. In a linear discontinuous region such as a region of contact discontinuity, the conventional TVD criterion is applied. In a nonlinear discontinuous region, e.g., a shock region, MLP limiter is used. Third, the regional information is fed into a flux scheme as well as a high order interpolation scheme. Based on this information, proper numerical dissipation is added to a nonlinear discontinuous region.

Through these ideas, e-MLP can contribute to the improvement of the solver in terms of accuracy, robustness and efficiency as follows. First, e-MLP can substantially enhance the solution accuracy due to the switching of the limiting criteria according to the features of the flow field; in a continuous region, there are no clipping phenomena since no limiting function is used. In a linear discontinuous region, excessive damping is removed by using the TVD criterion. And in a nonlinear discontinuous region, effective oscillation removal can be offered by the MLP limiter. As a result, e-MLP can include a

considerable amount of information pertaining to flow physics and can provide accurate solutions with the enhanced oscillation removal ability, especially in the event of a complex shock structure.

Second, due to the multi-dimensional search routine for discontinuities and due to the addition of proper numerical dissipation in a flux evaluation scheme, e-MLP is very robust against shock instability. In a conventional one-dimensional way of discontinuity searching, the existence of shock wave is determined one-dimensionally, which may bring forth in the numerical shock region if the shock is aligned with the grid system. Consequently, these slip phenomena may cause a density perturbation that acts as a source of instability in the numerical shock region and leads to bad convergence in a steady problem. On the other hand, in e-MLP, the perturbation can be easily damped out by help of the independent multi-dimensional search routine for discontinuities. The refined information from this routine is used when adding proper numerical dissipation to a nonlinear discontinuous region in a flux scheme. Especially, in complicated problems such as MHD flows, where the TVD criterion are not sufficient for oscillation removal even in one-dimensional cases, e-MLP is highly advantageous in shock instability.

Third, e-MLP increases the efficiency through a reduction of the necessary computational time. Generally, the majority of a computational domain is a smooth region with the exception of some discontinuous regions, where limiting criteria are necessary. In this situation, the application of a limiting function to the entire domain is a waste of computational resources. Thus, e-MLP can reduce the computational cost via the application of limiting functions only to a discontinuous region.

The overall process of e-MLP to realize the above mentioned idea is shown in Fig. 1.

Step 1. *Distinction of the computational domain*: For accurate distinction between continuous, linear discontinuous and nonlinear discontinuous regions, each type of region is searched multi-dimensionally by using the fourth order of polynomial interpolation and Gibbs phenomenon. The detail is explained in Section 4.

Step 2. *Higher order interpolation*: After the distinguishing step, an appropriate limiting function is applied to each type of region. In a continuous region, a limiting function is unnecessary and simple high order accurate interpolation is performed. In a linear discontinuous region, the conventional TVD criterion is applied for oscillation removal. Last, in a nonlinear discontinuous region, MLP limiter is used. The detail is explained in Section 5.

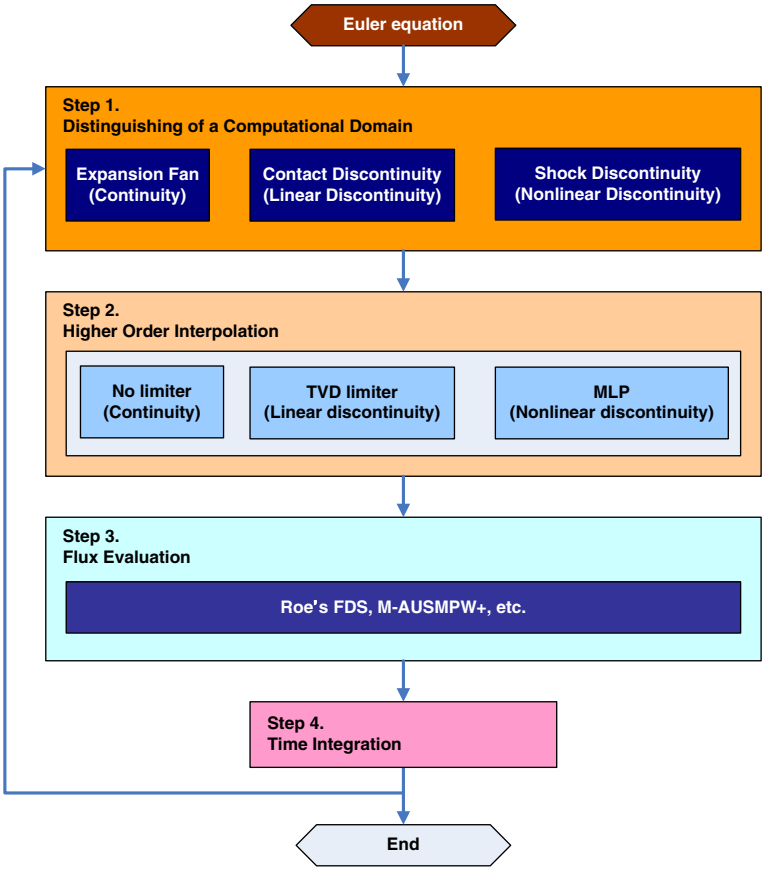

Fig. 1. Overall procedure of new limiting process.

Step 3. *Flux evaluation*: For flux scheme, e-MLP easily cooperates with any numerical scheme such as Roe's FDS [11], AUSMPW+/M-AUSMPW+ [12,13], etc. In the present paper, M-AUSMPW+ is mainly used as a flux scheme at cell-interfaces. In the case of a blunt body problem, Roe's FDS is used.

Step 4. *Time integration*: In e-MLP, any type of time integration scheme can be applied among implicit or explicit methods. In the present study, the third order of the Runge–Kutta scheme is used for time integration [14].

4. Distinguishing step

Differentiation between continuous and discontinuous regions has been one of the important issues in the CFD field for stable and effective oscillation removal. Most previous limiters, such as TVD, TVB, ENO and others were developed for this purpose based on rigorous one-dimensional scalar analyses and have been widely used for oscillation removal. Even though they show good characteristics in one-dimensional discontinuity, they do not provide so perfect performances in multi-dimensions as in one-dimension. Also, they cannot distinguish between linear and nonlinear discontinuities since they are based on scalar analyses. Moreover, because discontinuity search algorithms that they include are generally coupled with an interpolation scheme, it is not easy to present precise information about a discontinuity to a flux scheme. It is therefore recommended that the search routine is separated from an interpolation scheme to distinguish linear/nonlinear discontinuities multi-dimensionally.

4.1. Distinction between continuities and discontinuities

Mathematical distinction between continuity and discontinuity is definite and easy to understandable. However, it is hard to clearly distinguish between them in a discretized numerical computation. When an actually continuous profile is represented in a discretized domain, a numerical profile is not seen to be continuous any more if a mesh size is larger than some threshold value. On the other hand, a numerical discontinuity looks to be a continuous wave if numerical dissipation is so large that the discontinuity is smeared a lot. It is a fundamental problem in a discretized computation. Therefore, it is definitely necessary to introduce the new definition of numerical discontinuity which is affected by the mesh size. In the present paper, Gibbs phenomenon at the edges of discontinuity is used to newly define numerical discontinuity. The fourth order of central differencing scheme is selected as the sensing function to indicate whether or not the Gibbs phenomenon occurs from the given distribution. An approximated value $f_{approxi}$ is presented as Eq. (5).

$$f_{approxi,i} = \frac{-f_{i-2} + 4f_{i-1} + 4f_{i+1} - f_{i+2}}{6} = f_i + O(\Delta x^4). \tag{5}$$

In a continuous region, the difference at point i between an original value and an approximated value is derived as Eq. (6).

$$\text{In a continuous region, } d_i = \frac{|f_{approxi,i} - f_i|}{|f|_i} \cong O(\Delta x^4). \tag{6}$$

However, if the approximation is performed near a discontinuous region, Gibbs phenomena are easily observed around the edges of numerical discontinuities; these cause an interpolated plot to differ from the original distribution as shown in Fig. 2. Hence, the variation d_i is considerably larger than the order of $O(\Delta x^4)$, as in Eq. (7).

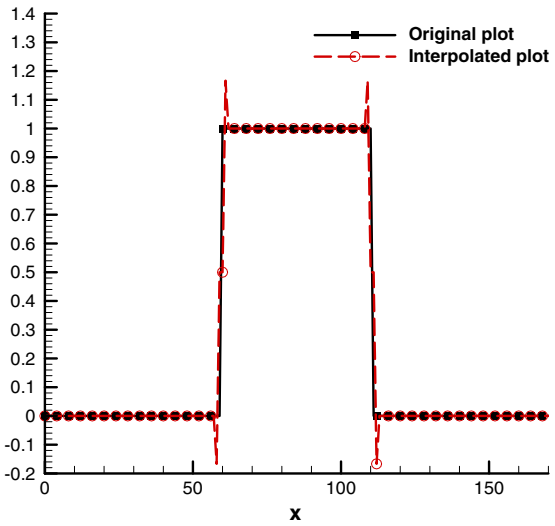

Fig. 2. An example of Gibbs phenomenon.

In a discontinuous region, $d_i \gg O(\Delta x^4)$. (7)

Therefore, it is thought that Gibbs phenomena are good criteria for numerically differentiating a discontinuous region from a continuous region. In the present paper, we introduce a threshold value, ε, to identify Gibbs phenomena and then define numerically continuous and discontinuous regions in the discretized domain. If $d_i \geqslant \varepsilon$, it is considered that Gibbs phenomena occur. Hence, the current region is determined as a numerically discontinuous region. Here, on a digital computer, a function is expressed by sets of discrete values; moreover, there are some losses of information when representing the original function. The losses may cause the region at which point the function rapidly changes to appear as a discontinuous region, not a continuous region any more, i.e., a rapidly varying region may share the Gibbs phenomena in the numerical computations. Therefore, a rapidly varying region as well as an actual discontinuity should be treated as a numerically discontinuous region in computations.

4.2. Distinction between linear and nonlinear discontinuities

Generally, the conventional TVD criterion is not sufficient for oscillation removal of Euler equations in multi-dimensional cases, while it is sufficient for one-dimensional case. Especially in MHD problems which contain many discontinuities and their interactions, it is disappointing even in one-dimensional flow problems. For effective oscillation removal in a nonlinear discontinuous region, a stricter limiting function is required. In contrast to a nonlinear discontinuous region, excessive damping by a strict limiting function may reduce the accuracy of the solution in a linear discontinuous region. Therefore, the types of discontinuities are necessary to be distinguished for appropriate switching of the limiting functions according to the type.

Inequalities of Eq. (8) are used to identify a linear contact discontinuity or a slip line. In the present paper, the same limiting function is used for both contact discontinuity and slip line because they share the condition that there is no pressure jump across them.

$$\begin{aligned} &d_{\rho,i} = \frac{|\rho_{approxi,i} - \rho_i|}{|\rho_i|} > \varepsilon \quad \text{or } d_{u,i} = \frac{|u_{approxi,i} - u_i|}{|u_i|} > \varepsilon, \\ &\text{and } d_{p,i} = \frac{|p_{approxi,i} - p_i|}{|p_i|} \approx O(\Delta x^4). \end{aligned} \tag{8}$$

where ρ, u, and p are non-dimensionalized density, velocity and pressure, respectively.

Inequalities of Eq. (9) serve to express a shock discontinuity.

$$\begin{aligned} &d_{\rho,i} = \frac{|\rho_{approxi,i} - \rho_i|}{|\rho_i|} > \varepsilon \quad \text{or } d_{u,i} = \frac{|u_{approxi,i} - u_i|}{|u_i|} > \varepsilon, \\ &\text{and } d_{p,i} = \frac{|p_{approxi,i} - p_i|}{|p_i|} > \varepsilon. \end{aligned} \tag{9}$$

Only if $d_p \geqslant \varepsilon$, the region is recognized as a nonlinear discontinuous region in the present paper. Here, there is always the possibility that $|u_i|$ is physically zero, different from $|\rho_i|$, $|p_i|$. In case that the magnitude of $|u_i|$ is almost zero, it is much probable that the point i is determined as a discontinuous region even though the region is actually a continuous region. In order to avoid this situation, the region is enforced to be a continuous region if $|u_i|$ is smaller than 10^{-6} in the present study.

In MHD problems, the sum of the thermal and magnetic pressure should be equal across a linear contact discontinuity. Hence, a nonlinear shock discontinuity for a MHD system can be checked by Eq. (10).

$$\begin{aligned} &d_{\rho,i} = \frac{|\rho_{approxi,i} - \rho_i|}{|\rho_i|} > \varepsilon \quad \text{or } d_{u,i} = \frac{|u_{approxi,i} - u_i|}{|u_i|} > \varepsilon, \\ &\text{and } d_{p,i} = \frac{|p_{tot,approxi,i} - p_{tot,i}|}{|p_{tot,i}|} > \varepsilon, \end{aligned} \tag{10}$$

where $p_{tot} = p + \mathbf{B}^2/2$.

By adjusting the check criteria, e-MLP can be extended to various types of physical problems.

4.3. Summary of distinguishing step

The distinguishing step can be simply extended to multi-dimensions by calculating the difference values in each direction, averaging them, and comparing the average with ε. For convenience, the summary of the distinguishing step are presented for two-dimensional cases.

Algorithm 1. Distinguishing step

$Itag_{i,j} = 0$; Continuous region
$Itag_{i,j} = 1$; Linear discontinuous region
$Itag_{i,j} = 2$; Nonlinear discontinuous region
$f_{i,j} = (\rho, u, v, p)_{i,j}$
do j=1 to $jmax$
do i=1 to $imax$

$$(d_{i,j})_i = \left| \frac{-\frac{1}{6}f_{i-2,j} + \frac{2}{3}f_{i-1,j} + \frac{2}{3}f_{i+1,j} - \frac{1}{6}f_{i+2,j}}{f_{i,j}} - 1 \right| \tag{11a}$$

$$(d_{i,j})_j = \left| \frac{-\frac{1}{6}f_{i,j-2} + \frac{2}{3}f_{i,j-1} + \frac{2}{3}f_{i,j+1} - \frac{1}{6}f_{i,j+2}}{f_{i,j}} - 1 \right| \tag{11b}$$

$$\bar{d}_{i,j} = \Big((d_{i,j})_i + (d_{i,j})_j \Big)/2. \tag{11c}$$

enddo
enddo
do j = 1 to $jmax$
do i = 1 to $imax$

$$Itag_i = 0$$

enddo
enddo
do j = 1 to $jmax$
do i = 1 to $imax$
  if $|\bar{d}_{\rho,i,j}| > \varepsilon$, then $Itag_i = 1$
  if $|u_{i,j}| \geqslant |v_{i,j}|$
    if $|\bar{d}_{u,i,j}| > \varepsilon$ and $|u_{i,j}| > 10^{-6}$ then $Itag_i = 1$
  else $|u_{i,j}| < |v_{i,j}|$
    if $|\bar{d}_{v,i,j}| > \varepsilon$ and $|v_{i,j}| > 10^{-6}$ then $Itag_i = 1$
  endif
  if $|\bar{d}_{p,i,j}| > \varepsilon$, then $Itag_i = 2$
enddo
enddo

5. Enhanced limiting process

In CFD, since the late 1970s, many researchers have tried to handle discontinuities without spurious oscillations. Important concepts for oscillation removal schemes include TVD, TVB, ENO and MLP. Each method has its own advantages and disadvantages, as shown in Table 1.

As shown in Table 1, there is no scheme that can deal with all three cases. In order to resolve this situation, the enhanced limiting process based on MLP in conjunction with the distinguishing step is proposed. In the enhanced limiting process, limiting functions are switched so that they are appropriate for each type of region, as Table 2.

The details are written in the following sections with the notation and theories of earlier studies [6,7] and [13].

Table 1
Comparison of advantage and disadvantage of various limiting functions.

	TVD	TVB, ENO	MLP
Discontinuity in one-dimension	O	O	O
Discontinuity in multi-dimensions	X	X	O
Local extrema	X	O	X

Table 2
Limiting function according to the types of regions.

Types of region	Continuous region	Numerical linear discontinuous region	Numerical nonlinear discontinuous region
Limiting function	No limiting function	TVD	MLP

5.1. Continuous region

A continuous region can be divided into local extrema and a monotonically increasing or decreasing region. In monotonically increasing or decreasing regions that are sufficiently continuous, the higher order interpolated value is not restricted by MLP limiter, i.e., it is independent of the usage of MLP limiter and the higher order accuracy is able to be obtained [6]. On the other hand, in local extrema, any limiting function should not be used to preserve the accuracy of solution. The application of TVD criterion or MLP limiter definitely results in clipping phenomena near local extrema. Therefore, no limiting function is recommended to be applied to a continuous region in e-MLP.

5.2. Numerical linear discontinuous region

Through the distinguishing process, a contact discontinuity belongs to a linear discontinuous region. In this region, the application of MLP limiter may make the discontinuity diffusive, which decreases the accuracy of the solution. Thus, the conventional TVD criterion is used for oscillation removal.

Let us assume that there are no velocity jumps across the linear discontinuity. Then, the continuity equation is simply written as Eq. (12).

$$\frac{\partial \rho}{\partial t}+\frac{\partial \rho u}{\partial x}+\frac{\partial \rho v}{\partial y}=0 \rightarrow \frac{\partial \rho}{\partial t}+u\frac{\partial \rho}{\partial x}+v\frac{\partial \rho}{\partial y}=0. \tag{12}$$

Here, if a contact discontinuity is not aligned with the grid system, it may smear by numerical dissipation. Then, the smeared contact discontinuous profile can be assumed as a linear planar wave. Hence, Eq. (13) can be obtained.

$$\frac{\partial \rho}{\partial x}\Big/\frac{\partial \rho}{\partial y}=const. \tag{13}$$

By combining Eqs. (12) and (13), Eq. (14) can be derived.

$$\frac{\partial \rho}{\partial t}+(u+v\cdot const)\frac{\partial \rho}{\partial x}=0. \tag{14}$$

The two-dimensional linear convection equation changes to the equivalent one-dimensional equation. The conventional TVD limiting function can provide monotonic distributions in a two-dimensional planar contact wave. Consequently, it is chosen as the oscillation removal function for a linear discontinuous region in e-MLP.

5.3. Nonlinear discontinuity

In previous research pertaining to MLP [6,7], it was reported that MLP is an appropriate oscillation removal scheme for multi-dimensional shock waves. Thus, MLP limiter is used in a nonlinear discontinuous region. A brief summary MLP is as follows.

$$\mathbf{\Phi}_L=\overline{\mathbf{\Phi}}_i+0.5\max\left(0,\min\left(\alpha_L\Delta\mathbf{\Phi}_{i+\frac{1}{2}},\alpha_L\Delta\mathbf{\Phi}_{i-\frac{1}{2}},\beta_L\Delta\mathbf{\Phi}_{i-\frac{1}{2}}\right)\right), \tag{15a}$$

$$\mathbf{\Phi}_R=\overline{\mathbf{\Phi}}_{i+1}-0.5\max\left(0,\min\left(\alpha_R\Delta\mathbf{\Phi}_{i+\frac{1}{2}},\alpha_R\Delta\mathbf{\Phi}_{i+\frac{3}{2}},\beta_R\Delta\mathbf{\Phi}_{i+\frac{3}{2}}\right)\right). \tag{15b}$$

where $\Delta\mathbf{\Phi}_{i-\frac{1}{2}j}=\overline{\mathbf{\Phi}}_{ij}-\overline{\mathbf{\Phi}}_{i-1j}$, $\Delta\mathbf{\Phi}_{i+\frac{1}{2}j}=\overline{\mathbf{\Phi}}_{i+1j}-\overline{\mathbf{\Phi}}_{ij}$, $\Delta\mathbf{\Phi}_{i+\frac{3}{2}j}=\overline{\mathbf{\Phi}}_{i+2j}-\overline{\mathbf{\Phi}}_{i+1j}$ and $\overline{\mathbf{\Phi}}$ means a cell averaged value.

Here, the coefficients $\beta_{L,R}$ enable high order accurate computations, which are given in Section 5.4. The values $\alpha_{L,R}$ are determined as Eqs. (16) and (17).

Along ξ-direction

$$\alpha_L=g\left[\frac{2\max\left(1,|r_{\xi,L}|\right)\times\left|\left(\mathbf{\Phi}_{ML}-\overline{\mathbf{\Phi}}_{ij}\right)\Big/\Delta\mathbf{\Phi}_{i+\frac{1}{2}j}\right|}{1+\max(0,\tan\theta_{\xi,ij})}\right], \tag{16a}$$

$$\alpha_R=g\left[\frac{2\max\left(1,|r_{\xi,R}|\right)\times\left|\left(\overline{\mathbf{\Phi}}_{i+1j}-\mathbf{\Phi}_{MR}\right)\Big/\Delta\mathbf{\Phi}_{i+\frac{1}{2}j}\right|}{1+\max(0,\tan\theta_{\xi,i+1j})}\right], \tag{16b}$$

where $g(x)=\max(1,\min(2,x))$, $r_{\xi,L}=\Delta\mathbf{\Phi}_{i+\frac{1}{2}j}\Big/\Delta\mathbf{\Phi}_{i-\frac{1}{2}j}$ and $r_{\xi,R}=\Delta\mathbf{\Phi}_{i+\frac{1}{2}j}\Big/\Delta\mathbf{\Phi}_{i+\frac{3}{2}j}$.

Along η-direction

$$\alpha_L = g\left[\frac{2\max\left(1,|r_{\eta,L}|\right)\times\left|\left(\mathbf{\Phi}_{ML}-\overline{\mathbf{\Phi}}_{ij}\right)/\Delta\mathbf{\Phi}_{i,j+\frac{1}{2}}\right|}{1+\max(0,\tan\theta_{\eta,i,j})}\right], \tag{17a}$$

$$\alpha_R = g\left[\frac{2\max\left(1,|r_{\eta,R}|\right)\times\left|\left(\overline{\mathbf{\Phi}}_{i+1,j}-\mathbf{\Phi}_{MR}\right)/\Delta\mathbf{\Phi}_{i,j+\frac{1}{2}}\right|}{1+\max(0,\tan\theta_{\eta,i,j+1})}\right], \tag{17b}$$

where $r_{\eta,L}=\Delta\mathbf{\Phi}_{i,j+\frac{1}{2}}\big/\Delta\mathbf{\Phi}_{i,j-\frac{1}{2}}$ and $r_{\eta,R}=\Delta\mathbf{\Phi}_{i,j+\frac{1}{2}}\big/\Delta\mathbf{\Phi}_{i,j+\frac{3}{2}}$.

$\alpha_{L\ or\ R}$ varies between 1 and 2, which controls the amount of numerical dissipation according to the maximum gradient angle of $\mathbf{\Phi}$ with a cell-interface, $\theta_{i,j}$. The angle, $\theta_{\xi,i,j}$ and $\theta_{\eta,i,j}$ mean the angle with a cell-interface $\left(i+\frac{1}{2},j\right)$ in ξ-direction and a cell-interface $\left(i,j+\frac{1}{2}\right)$ in η-direction defined as Eq. (18), respectively.

$$\tan\theta_{\xi,i,j}=\frac{\left|\overline{\mathbf{\Phi}}_{i,j+1}-\overline{\mathbf{\Phi}}_{i,j-1}\right|}{\left|\overline{\mathbf{\Phi}}_{i+1,j}-\overline{\mathbf{\Phi}}_{i-1,j}\right|}\quad\text{along }\xi-\text{direction}, \tag{18a}$$

$$\tan\theta_{\eta,i,j}=\frac{\left|\overline{\mathbf{\Phi}}_{i+1,j}-\overline{\mathbf{\Phi}}_{i-1,j}\right|}{\left|\overline{\mathbf{\Phi}}_{i,j+1}-\overline{\mathbf{\Phi}}_{i,j-1}\right|}\quad\text{along }\eta-\text{direction}. \tag{18b}$$

The zero of $\theta_{i,j}$ means that the distribution of $\mathbf{\Phi}$ is perfectly aligned with a grid system. Then, α has the value of 2 and MLP limiter becomes the same as TVD criterion. On the other hand, if $\theta_{i,j}$ is 45°, α approaches 1 and numerical dissipation increases [6]. The values of $\mathbf{\Phi}_{ML}$ and $\mathbf{\Phi}_{MR}$ in Eqs. (16) and (17) mean the maximum and minimum values within the region, $i<m<i+1$ and $j-1<n<j+1$, at the cell-interface $\left(i+\frac{1}{2},j\right)$ in ξ-direction or the region, $i-1<m<i+1$ and $j<n<j+1$, at the cell-interface $\left(i,j+\frac{1}{2}\right)$ in η-direction defined as Eq. (19). The interpolated values $\mathbf{\Phi}_L$ and $\mathbf{\Phi}_R$ at the cell-interface must be between them.

Along ξ-direction

$$\mathbf{\Phi}_{ML}=\max(\mathbf{\Phi}_{m,n}),\quad \mathbf{\Phi}_{MR}=\min(\mathbf{\Phi}_{m,n})\quad\text{where }\Delta\mathbf{\Phi}_{i+\frac{1}{2}j}>0,\quad i<m<i+1\quad\text{and }j-1<n<j+1. \tag{19a}$$

$$\mathbf{\Phi}_{ML}=\min(\mathbf{\Phi}_{m,n}),\quad \mathbf{\Phi}_{MR}=\max(\mathbf{\Phi}_{m,n})\quad\text{where }\Delta\mathbf{\Phi}_{i+\frac{1}{2}j}\leqslant 0,\quad i<m<i+1\quad\text{and }j-1<n<j+1. \tag{19b}$$

Along η-direction

$$\mathbf{\Phi}_{ML}=\max(\mathbf{\Phi}_{m,n}),\quad \mathbf{\Phi}_{MR}=\min(\mathbf{\Phi}_{m,n})\quad\text{where }\Delta\mathbf{\Phi}_{ij+\frac{1}{2}}>0,\quad i-1<m<i+1\quad\text{and }j<n<j+1. \tag{19c}$$

$$\mathbf{\Phi}_{ML}=\min(\mathbf{\Phi}_{m,n}),\quad \mathbf{\Phi}_{MR}=\max(\mathbf{\Phi}_{m,n})\quad\text{where }\Delta\mathbf{\Phi}_{ij+\frac{1}{2}}\leqslant 0,\quad i-1<m<i+1\quad\text{and }j<n<j+1. \tag{19d}$$

In implementing e-MLP into a code, very small value (10^{-16}) is added to a denominator.

5.4. Summary of the enhanced Multi-dimensional Limiting Process

In summary, the enhanced Multi-dimensional Limiting Process (e-MLP) with high order accuracy is as follows according to different regions.

(1) Continuous region: No limiting function

$$\mathbf{\Phi}_L=\overline{\mathbf{\Phi}}_i+0.5\beta_L\Delta\mathbf{\Phi}_{i-\frac{1}{2}}, \tag{20a}$$

$$\mathbf{\Phi}_R=\overline{\mathbf{\Phi}}_{i+1}-0.5\beta_R\Delta\mathbf{\Phi}_{i+\frac{3}{2}}. \tag{20b}$$

(2) Linear discontinuous region: TVD criterion, $\phi(r)$ = max (0,min (2,2r))

$$\mathbf{\Phi}_L=\overline{\mathbf{\Phi}}_i+0.5\max\left(0,\min\left(2\Delta\mathbf{\Phi}_{i+\frac{1}{2}},2\Delta\mathbf{\Phi}_{i-\frac{1}{2}},\beta_L\Delta\mathbf{\Phi}_{i-\frac{1}{2}}\right)\right), \tag{21a}$$

$$\mathbf{\Phi}_R=\overline{\mathbf{\Phi}}_{i+1}-0.5\max\left(0,\min\left(2\Delta\mathbf{\Phi}_{i+\frac{1}{2}},2\Delta\mathbf{\Phi}_{i+\frac{3}{2}},\beta_R\Delta\mathbf{\Phi}_{i+\frac{3}{2}}\right)\right). \tag{21b}$$

(3) Nonlinear discontinuous region: MLP limiter, $\phi(r)$ = max (0,min (α,αr))

$$\mathbf{\Phi}_L=\overline{\mathbf{\Phi}}_i+0.5\max\left(0,\min\left(\alpha_L\Delta\mathbf{\Phi}_{i+\frac{1}{2}},\alpha_L\Delta\mathbf{\Phi}_{i-\frac{1}{2}},\beta_L\Delta\mathbf{\Phi}_{i-\frac{1}{2}}\right)\right), \tag{22a}$$

$$\mathbf{\Phi}_R=\overline{\mathbf{\Phi}}_{i+1}-0.5\max\left(0,\min\left(\alpha_R\Delta\mathbf{\Phi}_{i+\frac{1}{2}},\alpha_R\Delta\mathbf{\Phi}_{i+\frac{3}{2}},\beta_R\Delta\mathbf{\Phi}_{i+\frac{3}{2}}\right)\right). \tag{22b}$$

The definitions of $\beta_{L,R}$ for the third order accurate and the fifth order accurate computations are presented in Eqs. (23) and (24), respectively.

e-MLP with third order accuracy (e-MLP3):

$$\beta_L \Delta\overline{\mathbf{\Phi}}_{i-\frac{1}{2}j} = -\frac{1}{3}\overline{\mathbf{\Phi}}_{i-1j} - \frac{1}{3}\overline{\mathbf{\Phi}}_{ij} + \frac{2}{3}\overline{\mathbf{\Phi}}_{i+1j}, \tag{23a}$$

$$\beta_R \Delta\overline{\mathbf{\Phi}}_{i+\frac{3}{2}j} = \frac{1}{3}\overline{\mathbf{\Phi}}_{i+2j} + \frac{1}{3}\overline{\mathbf{\Phi}}_{i+1j} - \frac{2}{3}\overline{\mathbf{\Phi}}_{ij}. \tag{23b}$$

e-MLP with fifth order accuracy (e-MLP5):

$$\beta_L \Delta\overline{\mathbf{\Phi}}_{i-\frac{1}{2}j} = \frac{2}{30}\overline{\mathbf{\Phi}}_{i-2j} - \frac{13}{30}\overline{\mathbf{\Phi}}_{i-1j} - \frac{13}{30}\overline{\mathbf{\Phi}}_{ij} + \frac{27}{30}\overline{\mathbf{\Phi}}_{i+1j} - \frac{3}{30}\overline{\mathbf{\Phi}}_{i+2j}, \tag{24a}$$

$$\beta_R \Delta\overline{\mathbf{\Phi}}_{i+\frac{3}{2}j} = -\frac{2}{30}\overline{\mathbf{\Phi}}_{i+3j} + \frac{13}{30}\overline{\mathbf{\Phi}}_{i+2j} + \frac{13}{30}\overline{\mathbf{\Phi}}_{i+1j} - \frac{27}{30}\overline{\mathbf{\Phi}}_{ij} + \frac{3}{30}\overline{\mathbf{\Phi}}_{i-1j}. \tag{24b}$$

Based on the appropriate application of the limiting functions, the oscillation behavior can be effectively removed. Moreover, better efficiency can be obtained because TVD criterion and MLP limiter are applied only to discontinuous regions.

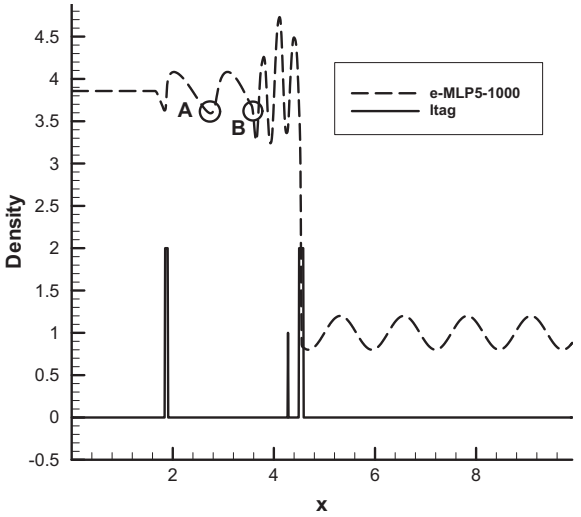

Fig. 3. Distinguished regions and density contour in shock/sine wave interaction problem.

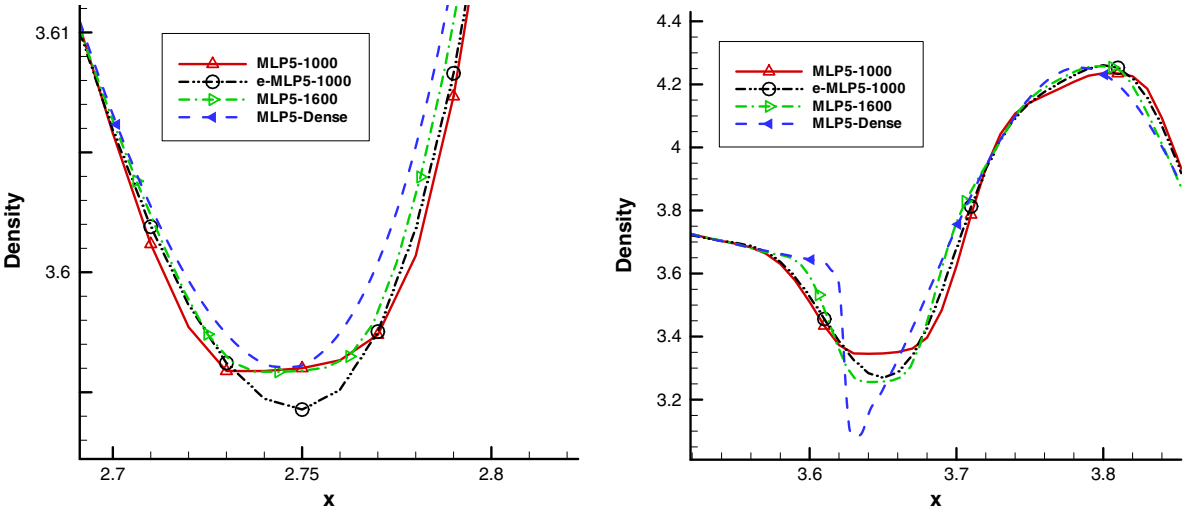

Fig. 4. Detailed comparison of density distribution in shock/sine wave interaction problem.

6. Numerical results

In order to investigate the actual features of e-MLP, it was applied to several test cases and its results were compared with those of MLP. The cases included one-dimensional shock/sine wave interaction problem, oblique stationary contact discontinuity, isentropic vortex flow, high speed flow in a blunt body, planar shock/density bubble interaction, normal shock wave/vortex interaction, and magnetohydrodynamic cloud-shock interaction problems. As e-MLP is independent of a flux scheme, essentially any numerical flux function can be adopted. In the present paper, Roe's FDS scheme and AUSMPW+/M-AUSMPW+ scheme were combined with MLP and e-MLP with the fifth order accuracy. In addition, the third order of the Runge–Kutta method was used as a time integration method. Here, an adequate range of the threshold value was $0.001 \leqslant \varepsilon \leqslant 0.01$ based on the vast amount of numerical tests that were run here; if $\varepsilon > 0.01$, a detrimental influence may ensue on the stability of the computations. Generally recommended ε values are 0.001 for steady problems or problems with fine grid points and 0.01 for other cases.

6.1. One-dimensional shock/sine wave interaction problem

In order to assess how well the distinguishing process of e-MLP divides the whole computational region into continuous, linear discontinuous and nonlinear discontinuous regions, e-MLP5 and MLP5 with M-AUSMPW+ were applied to one-dimensional shock/sine wave interaction problem. The initial conditions for shock-sine wave interaction problem are given as Eq. (25) [15].

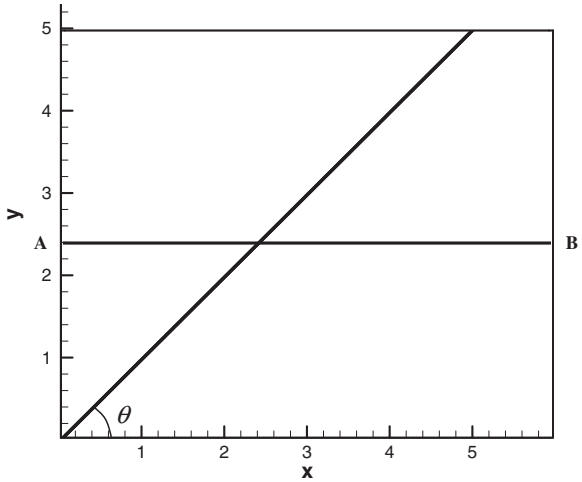

Fig. 5. Density contour of oblique stationary contact discontinuity (45°).

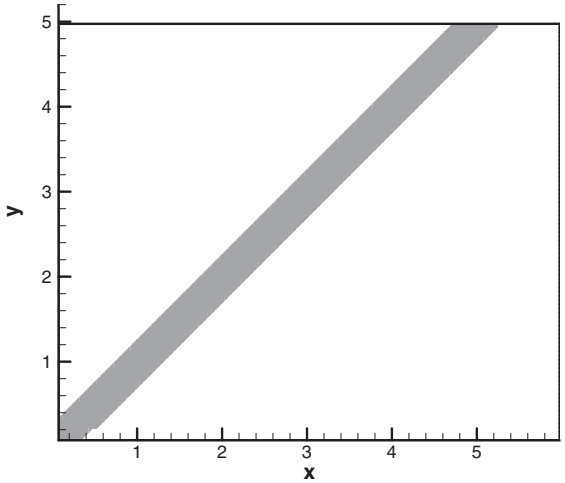

Fig. 6. Distinguished regions in oblique stationary contact discontinuity (45°) (□: Continuity, ▨: Linear discontinuity, ■: Nonlinear discontinuity).

$$(\rho, U, p) = (3.8571, 2.6294, 10.333) \quad \text{where } 0 \leqslant x \leqslant 1,$$
$$(\rho, U, p) = (1 + 0.2\sin(5(x-5)), 0, 1) \quad \text{where } 1 \leqslant x \leqslant 10. \tag{25}$$

Since the test case is one-dimensional problem, MLP limiter is the same as the TVD criterion, $\phi(r) = \max(0, \min(2, 2r))$, i.e. α_L and α_R values are always 2. Thus, the results of MLP5 always followed the typical features of TVD schemes. For comparing the results between MLP5 and e-MLP5, we used 1000 grid points. The reference result was calculated by using 10000 grid points with MLP5 and called as MLP5-dense. For flux evaluation and time integration, M-AUSMPW+ and the third order of Runge–Kutta method were used, individually.

Through the distinguishing process of e-MLP, the most regions were recognized as continuous regions except some discontinuous regions as in Fig. 3. Detailed density contours of MLP5 and e-MLP5 at t = 1sec are shown in Fig. 4. The result of e-MLP5 shows no clipping phenomenon at the extrema, different from that of MLP5. Moreover, the distribution of e-MLP5-1000 is similar to that of MLP5-1600 (MLP5 with 1600 grid points). Because the region around the extrema was determined as a continuous region in e-MLP, no limiting function was applied to the fifth order interpolated value, which could reduce the calculation time as well as increase accuracy.

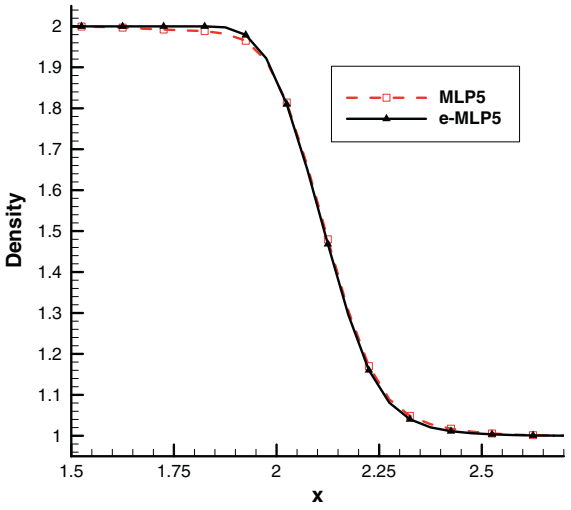

(a) Density distribution

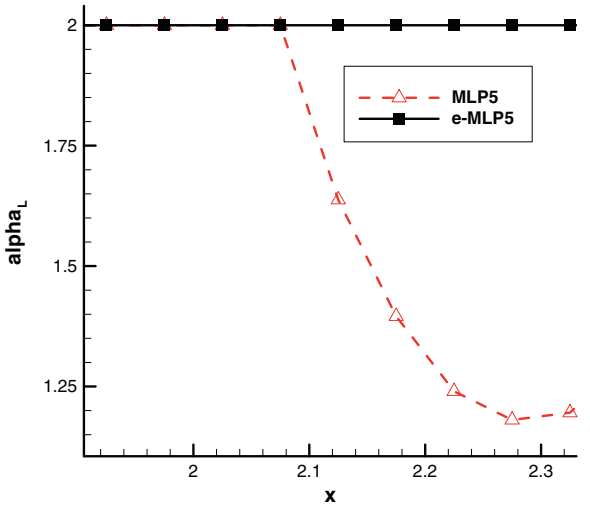

(b) α_L distribution

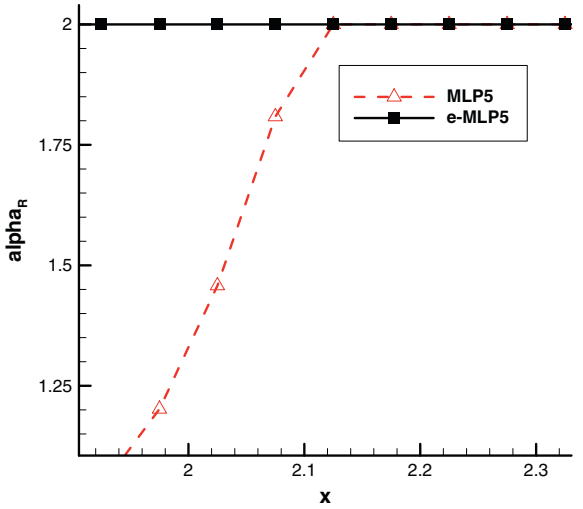

(c) α_R distribution

Fig. 7. Density and α distribution along line A–B (30°).

6.2. Oblique stationary contact discontinuity

In order to examine the adequacy of e-MLP compared with MLP in a contact discontinuity problem, an oblique stationary contact discontinuity was considered. The initial conditions are presented as Eq. (26).

$$(\rho_L, u_L, v_L, p_L) = \left(2.0, 0.1, 0.1\tan\theta, \frac{1}{\gamma}\right) \quad \text{and} \quad (\rho_L, u_L, v_L, p_L) = \left(1.0, 0.1, 0.1\tan\theta, \frac{1}{\gamma}\right). \tag{26}$$

The initial distribution inclined by θ degrees was shown in Fig. 5. The grid system was 121×101 and ε was 0.001 in this problem. For boundary conditions, free stream values were specified along the left and the bottom boundary, and extrapolations were used from the inside domain at the other boundaries. Furthermore, M-AUSMPW+ and the third order of the Runge–Kutta method were used for flux evaluation and time integration respectively.

In this problem, most of the computational domain was continuous except the region near the contact discontinuity. As was expected, e-MLP successfully divided the domain into continuous and linear discontinuous regions, as expressed in Fig. 6. Figs. 7 and 8 illustrate the density and α distributions of MLP5 and e-MLP5 along line A–B at 30° and 45°, respectively. These figures show that the density distributions of MLP5 are somewhat damped out compared to those of e-MLP5. It is

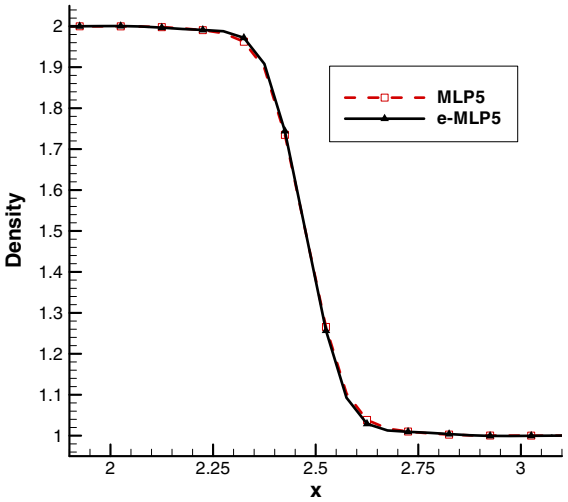

(a) Density distribution

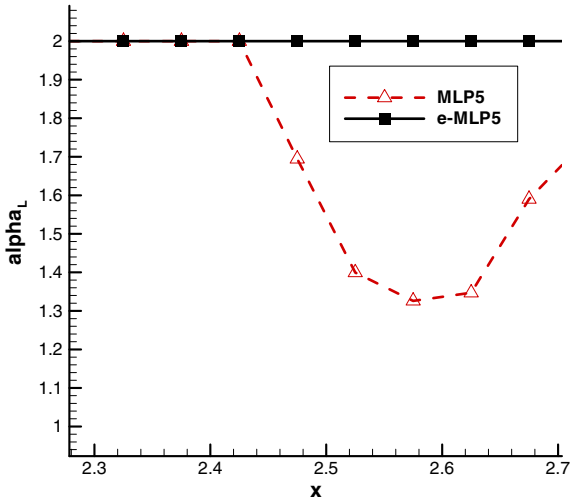

(b) α_L distribution

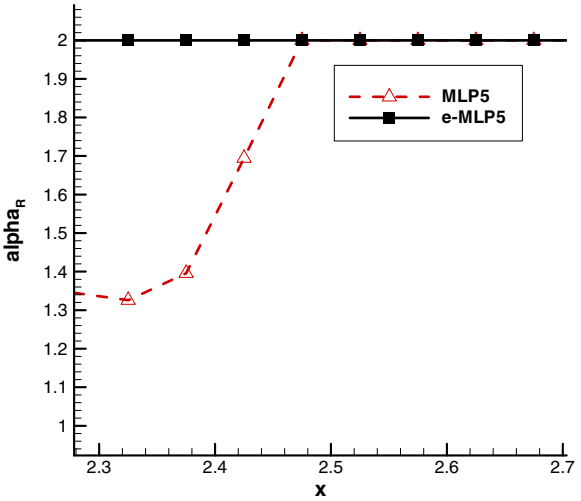

(c) α_R distribution

Fig. 8. Density and α distribution along line A–B (45°).

because the α values changes across the numerical contact discontinuity and they are always smaller than 2, which indicates that excessive damping occurs in the case of MLP5. However, in e-MLP5, the conventional TVD criterion is applied instead of MLP limiter; i.e., α values are fixed as 2 across the discontinuity. Hence, the improved steepness was obtained and the convergence rate was enhanced substantially in the case of e-MLP5, as shown in Fig. 9. Moreover, the computational time of MLP5 and e-MLP5 was 582.97 s and 342.97 s respectively; i.e., e-MLP5 was nearly 1.7 times faster than MLP5. It is expected that e-MLP enhances both accuracy and efficiency in a problem with a contact discontinuity.

6.3. Isentropic vortex flow

In order to assess the advantage of e-MLP in continuous problems of Euler equations, MLP5 and e-MLP5 were applied to an isentropic vortex flow problem. A vortex flow is a pure multi-dimensional phenomenon that is characterized by the existence of a negative pressure gradient toward the core. The curved flow contours and computed results are very sensitive to the choice of the interpolation and/or numerical fluxes. The vortex model is the isentropic vortex model defined as Eq. (27) [16].

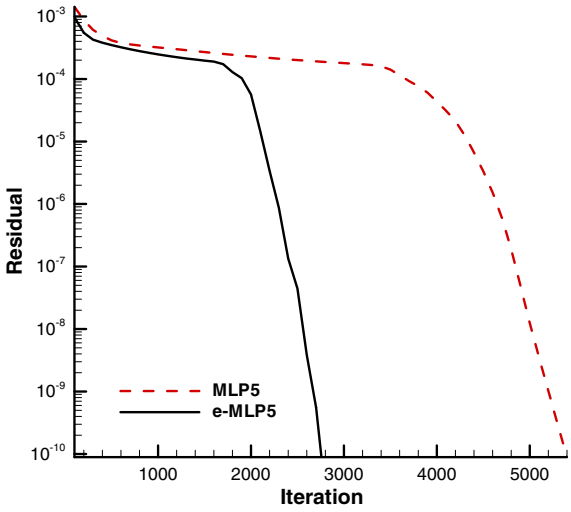

Fig. 9. Convergence histories of the oblique stationary contact discontinuity (45°).

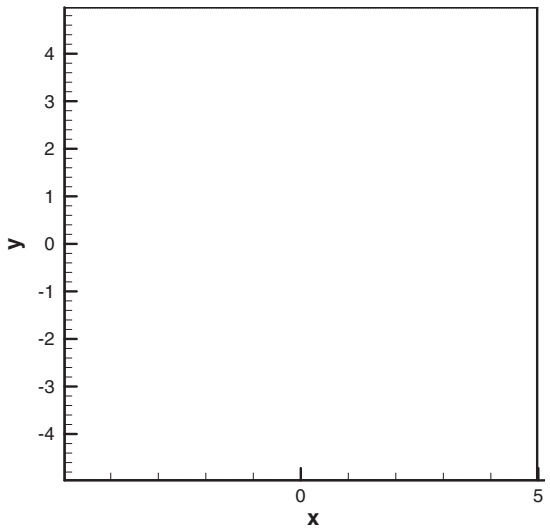

Fig. 10. Distinguished regions in an isentropic vortex problem (□: Continuity, ▒: Linear discontinuity, ■: Nonlinear discontinuity).

$$\text{Tangential velocity: } u_\theta = M_v r \exp\left[\frac{1-r^2}{2}\right], \tag{27a}$$

$$\text{Radial velocity: } u_r = 0, \tag{27b}$$

$$\text{Density velocity: } \rho(r) = \left(1 - \frac{\gamma-1}{2} M_v^2 \exp[1-r^2]\right)^{1/(\gamma-1)}, \tag{27c}$$

$$\text{Pressure distribution: } p(r) = \rho^\gamma/\gamma. \tag{27d}$$

Here, the computational domain ranged from $(-5,-5)$ to $(5,5)$ with equal grid spacing and the vortex core was located at $(0,0)$. The vortex Mach number, M_v was 1.0 and the number of grid points was 101×101. The CFL number was 0.5 and the boundary was fixed with initial values. Moreover, M-AUSMPW+ and the third order of the Runge–Kutta time integration were applied. The density distributions were plotted at a non-dimensional time of 80.

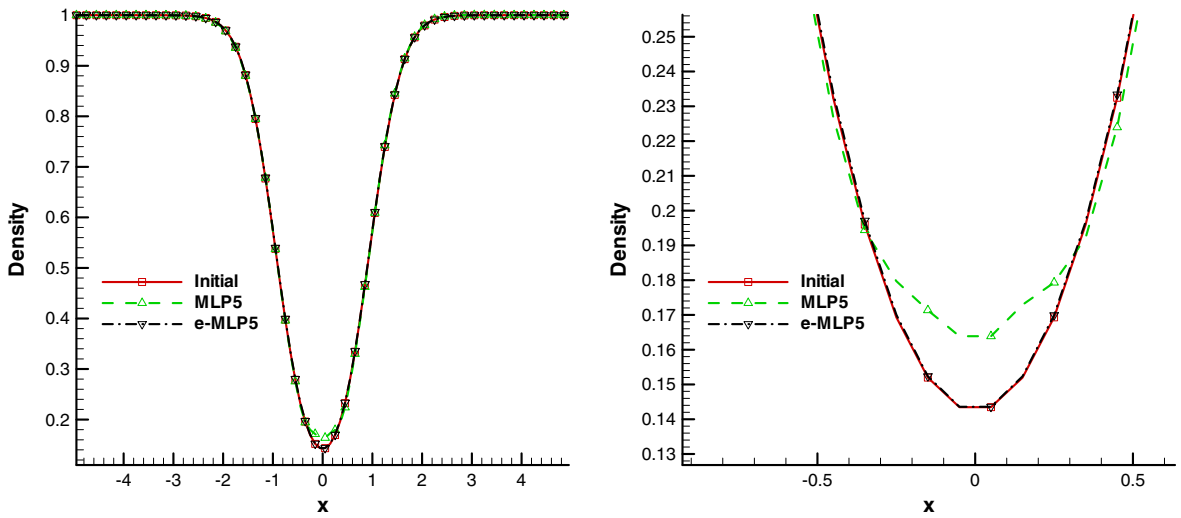

(a) Density distribution at $y = 0$ (b) Detailed density distribution at vortex core

Fig. 11. Comparison of density distributions in an isentropic vortex flow.

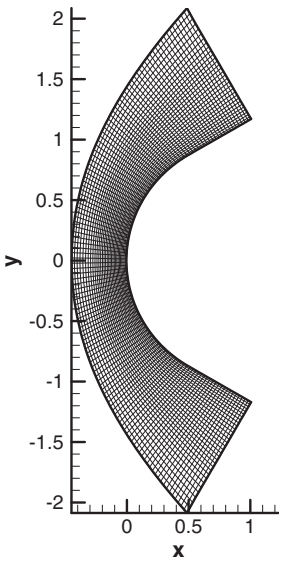

Fig. 12. Grid system for the high speed flow in a blunt body.

Through the distinguishing process with $\varepsilon = 0.01$, the whole computational domain was recognized as continuous regions, as shown in Fig. 10. Because any limiting function was not applied in e-MLP5, the computation of e-MLP5 (501.6 s) became faster than MLP5 (640.5 s); the overall computational time was reduced by 21.7%.

In Fig. 11, density distributions of MLP5 and e-MLP5 at y=0 are compared with the exact solution. Throughout the time marching process from the same exact solution, it is seen that MLP5 cannot maintain the initial distribution of the isentropic vortex flow and the density distribution does not seem to be symmetry because of the clipping phenomena at the vortex core. On the other hand, e-MLP5 preserves the initial exact solution well since the whole computational domain is determined as a continuous region and any limiting function is not applied in e-MLP. Through this test, e-MLP shows a considerable enhancement of accuracy in the continuous region including the local extrema comparing with MLP.

6.4. High speed flow in a blunt body

In a strong shock discontinuity, shock instability quite often occurs, which has a detrimental effect on the stability and convergence of solutions. In order to resolve this problem, the entropy fixing method is generally used in Roe's FDS, which is correspondent to the addition of numerical dissipation to any problematic regions [17,18]. However, the addition of

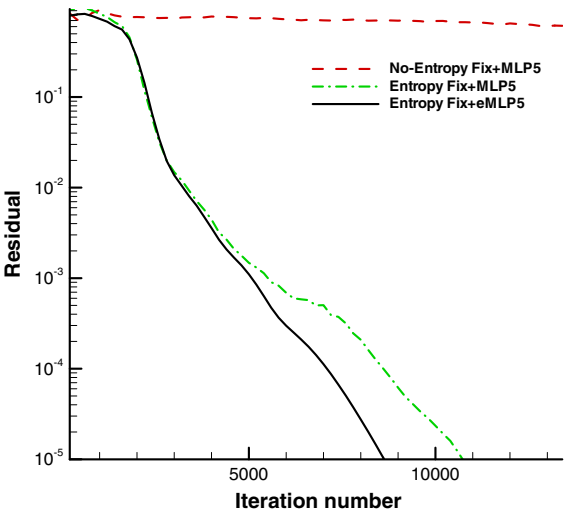

Fig. 13. Convergence histories of the high speed flow in a blunt body.

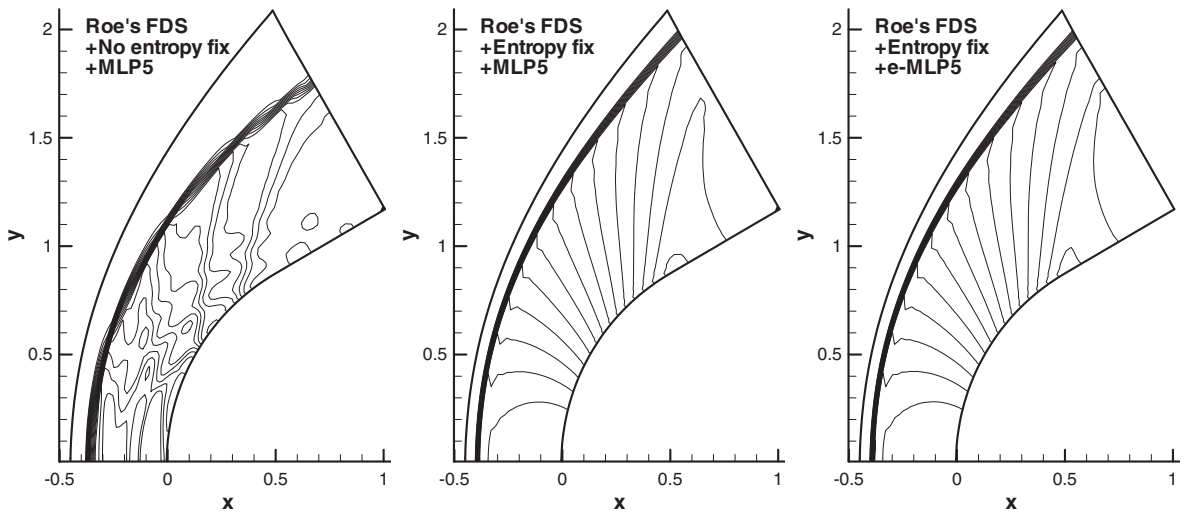

(a) No entropy fix+MLP5 (b) Entropy fix+MLP5 (c) Entropy fix+e-MLP5

Fig. 14. Comparison of pressure contours of high speed flow in a blunt body.

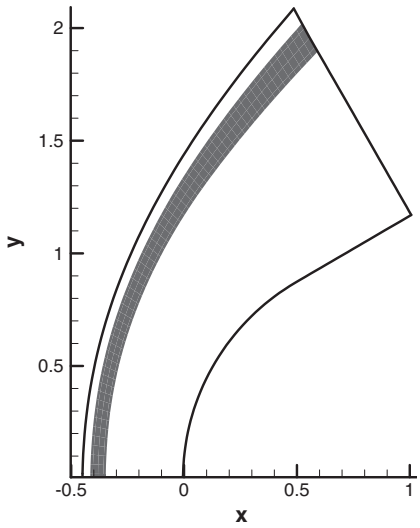

Fig. 15. Distinguished regions in high speed flow in a blunt body (□: Continuity, ▭: Linear discontinuity, ■: Nonlinear discontinuity).

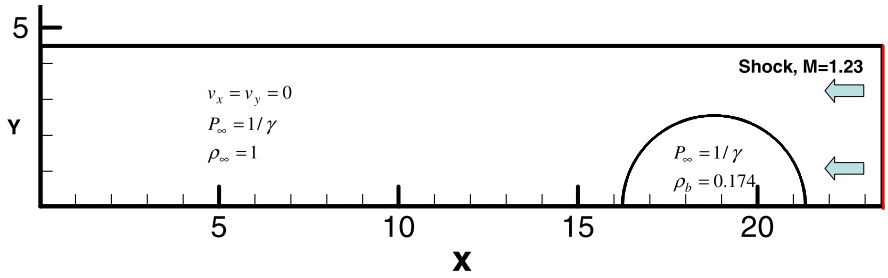

Fig. 16. Schematics of the problem definition of planar shock/density bubble interaction.

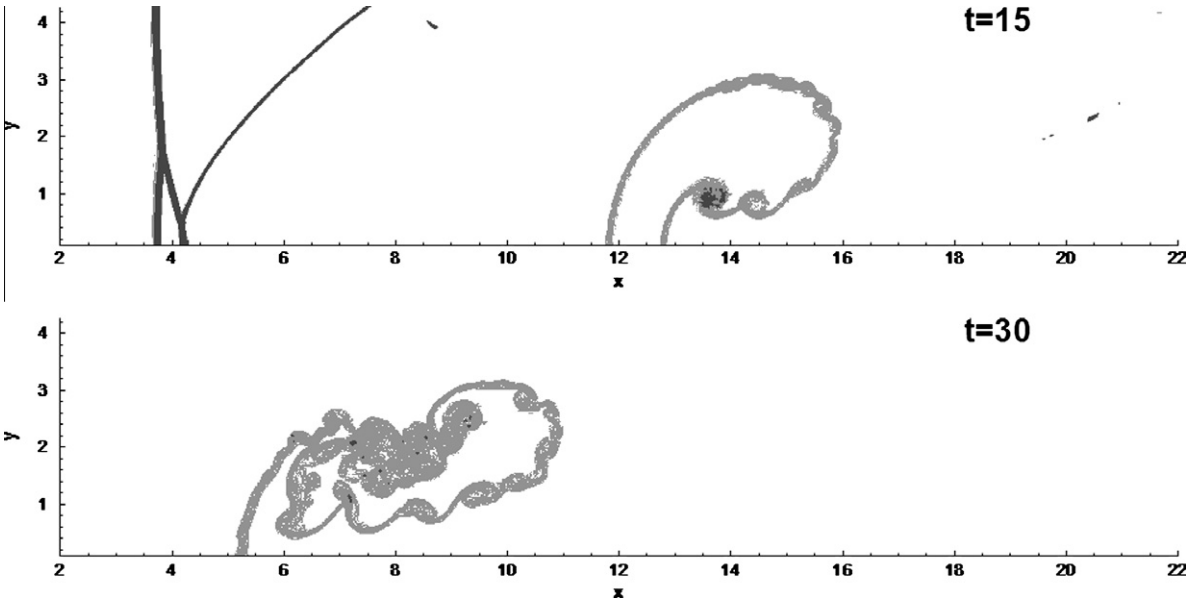

Fig. 17. Distinguished regions of planar shock/density bubble interaction (□: Continuity, ▭: Linear discontinuity, ■: Nonlinear discontinuity).

dissipation over the entire computational domain can decrease the accuracy and convergence of the solution, especially in the hypersonic boundary layer region. If Roe's FDS is applied to a hypersonic blunt body problem, the large amount of entropy fix may be necessary and has to be accurately applied only to a strong shock region. If it is applied in a boundary layer region, it is much probable that the solution is contaminated. To avoid this, there are several variations of entropy fix for Roe's FDS such as Eq. (28). In light of this, e-MLP can provide a viable solution in such a case due to its capability to divide the computational domain in a highly accurate manner.

To assess the e-MLP method in the event of a strong shock problem, it was applied to a high speed flow problem in a blunt body. The number of grid points was 127×35 and the grid system was well aligned with the shock, as shown in Fig. 12. The

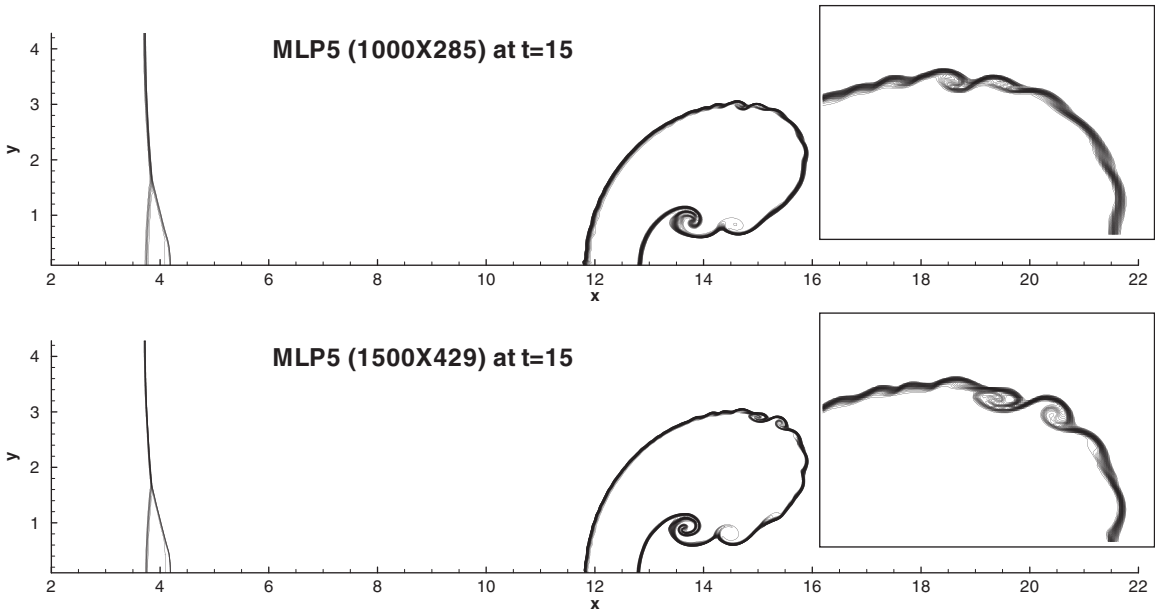

(a) MLP5 at t=15

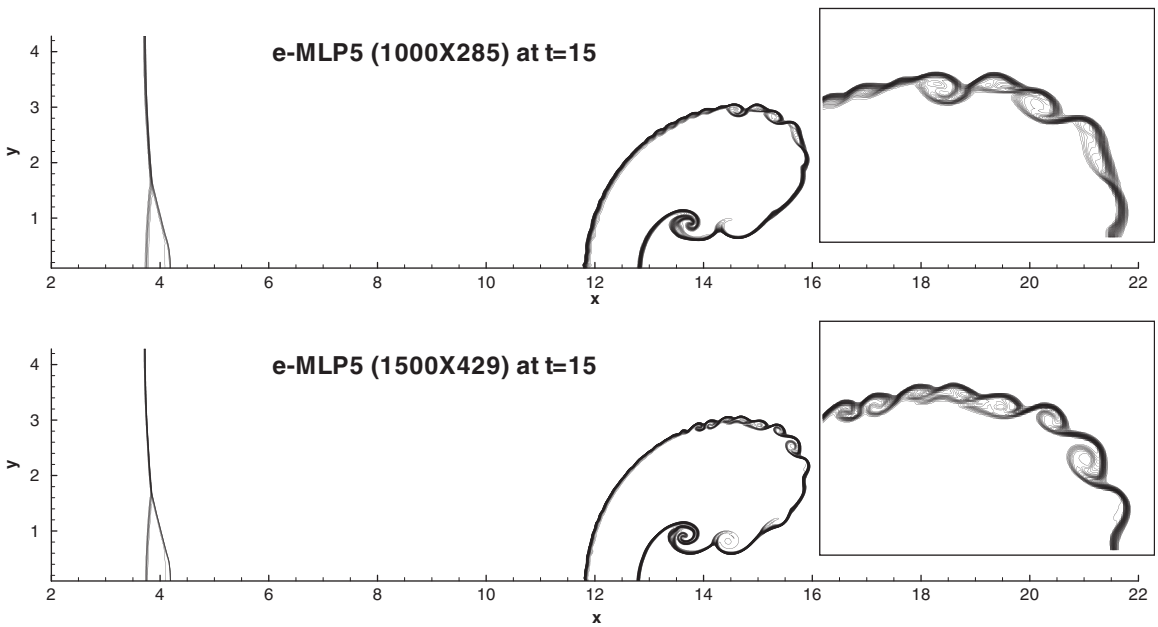

(b) e-MLP5 at t=15

Fig. 18. Comparison of density contours of planar shock/density bubble interaction.

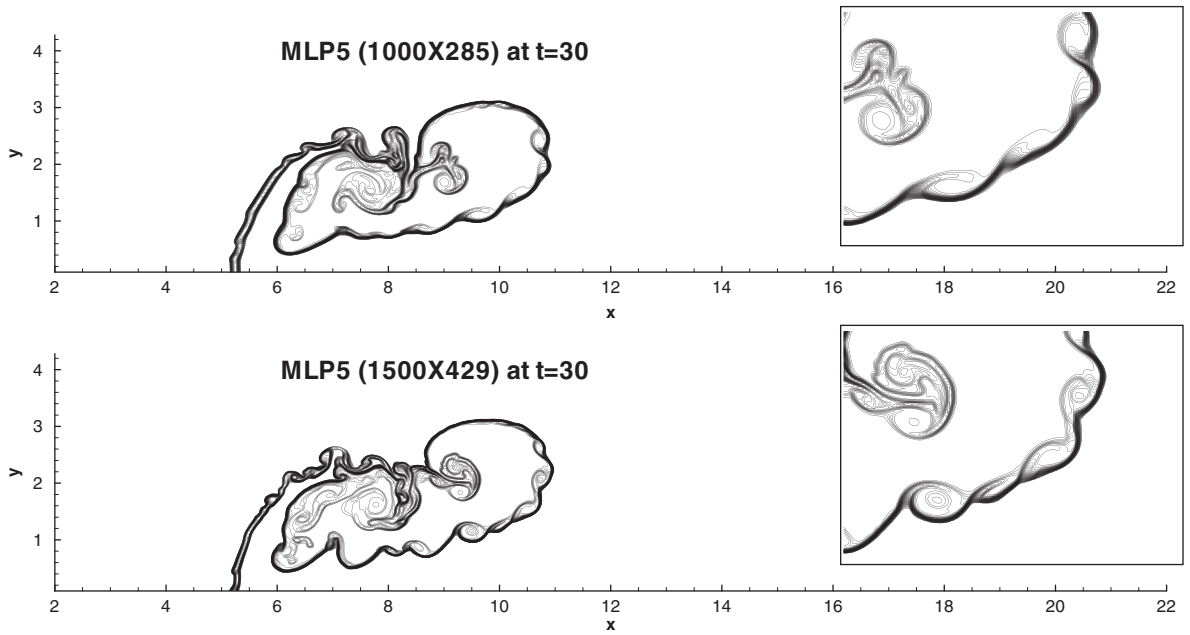

(c) MLP5 at t=30

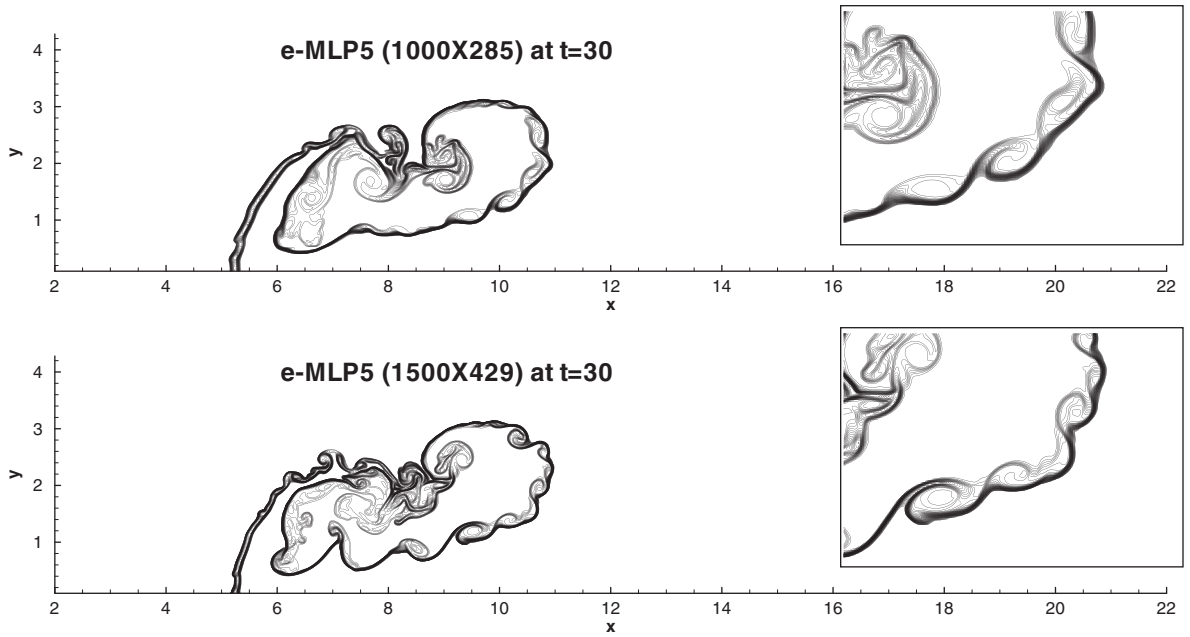

(d) e-MLP5 at t=30

Fig. 18 (*continued*)

free stream Mach number was 2.94 and the CFL number was 0.2. The Harten–Yee Entropy fixing method was used for the entropy fix, as expressed by Eq. (28) [18].

$$|\lambda| = \begin{cases} |\lambda| & \text{if } |\lambda| \geqslant \delta \\ (\lambda^2 + \delta^2)/(2\delta), & \text{if } |\lambda| < \delta \end{cases}, \tag{28a}$$

$$\delta = \delta^* \left[|\overline{W}_\xi| + |\overline{W}_\eta| + 0.5c\left(\left| \nabla \frac{\xi}{J} \right| + \left| \nabla \frac{\eta}{J} \right| \right) \right], \tag{28b}$$

where, $\overline{W}_\xi, \overline{W}_\eta$ are the contravariant velocities in the ξ and η directions, individually. The range of δ^* is $0.05 \leqslant \delta^* \leqslant 0.25$; the value of 0.05 was used in this calculation. For the wall boundary condition, an adiabatic wall condition was used. The temperature of free stream was 273 K. Roe's FDS and the third order of the Runge–Kutta methods are used for flux evaluation and time integration, respectively.

Figs. 13 and 14 show a comparison of the convergence histories and pressure contours for No entropy fix + MLP5, Entropy fix + MLP5 and Entropy fix + e-MLP5. In the case of No entropy fix + MLP5, numerical problems due to shock instability occurred as shown in Fig. 14(a), even if it did not progress toward the typical carbuncle phenomenon. In case of Entropy fix + MLP5, the additional numerical dissipation seemed to be sufficient for removal of the shock instability and the solution was converged. However, the α values in MLP limiter varied throughout the whole domain, which relatively worsened the convergence. In case of Entropy fix + e-MLP5, the strong shock discontinuous region was checked as a nonlinear discontinuous region and other regions were considered as a continuous region with $\varepsilon = 0.01$, as shown in Fig. 15. The calculations of α of MLP limiter and the entropy fix were therefore only imposed on the strong shock discontinuous region, which guaranteed the stable shock capturing with the better convergence. Through the enhanced convergence and the lessened time for the complicated computation of MLP limiter and the entropy fix method, the overall computational time was reduced from 661.91 s to 412.63 s, i.e., a reduction of 38% of the computational cost was gained through the use of e-MLP.

6.5. Planar shock/density bubble interaction

In order to show the accuracy enhancement of linear discontinuity in e-MLP, MLP and e-MLP were applied to the planar shock/density bubble interaction problem [19]. The computational domain ranged from (0,0) to (23.5,4.45) with 1000×285 and 1500×429 grid systems. A cylindrical density bubble was located at (18.8,0) with the diameter of 5.1. A normal shock with Mach number = 1.23 was moving from the right boundary to the left boundary and interacted with the bubble. For boundary conditions, Euler wall boundary condition and the symmetry boundary condition were applied to the upper and the lower boundaries, respectively. And outflow and inflow conditions were implemented to the left and the right boundaries. Here, M-AUSMPW+ and the third order of Runge–Kutta method were used for the computations. The schematic of problem definition is shown in Fig. 16.

At the non-dimensional time of 15 and 30 with $\varepsilon = 0.001$, the distinguished regions are shown in Fig. 17. The shock region and the boundaries of bubble were well divided as nonlinear and linear discontinuous regions, which verified that the distinguishing process in e-MLP worked successfully. Due to the distinguishing of computational domain, the computational time decreased from 14400 s to 12100 s with the 1000×285 grid system. In case of the 1500×429 grid system, the time was reduced from 42900 s to 36700 s, i.e., about 17% reduction of the overall computational time was obtained.

Fig. 18 shows the density contours of MLP5 and e-MLP5 at the non-dimensional time of 15 and 30. After interactions between a shock wave and a contact discontinuity, the complex evolution of vortex is frequently observed due to flow instability at a linear contact discontinuity. In computation, the vortices can be clearly represented as numerical dissipation decreases. The bubble in the 1500×429 grid system shows flow instability more definitely than that in the 1000×285 grid system. In the result of MLP5, relatively excessive numerical dissipation by MLP limiting function was introduced in linear contact discontinuities and it quite damped out the physical flow instability. It is clearly seen in Fig. 18(a) and (c) that the instability of MLP5 is delayed. Due to this delay, MLP5 generated the less developed vortex pattern than e-MLP5 at the time

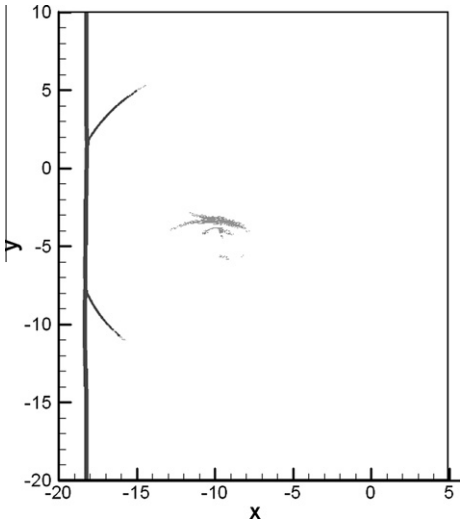

Fig. 19. Distinguished regions in normal shock wave/vortex interaction flow (□: Continuity, ▨: Linear discontinuity, ■: Nonlinear discontinuity).

of 30. Based on this test, it is confirmed again that the distinction of linear discontinuity from nonlinear discontinuity and the proper selection of limiting function may lead to the enhancement in accuracy as well as in efficiency.

6.6. Normal shock wave/vortex flow interaction

In order to ascertain the advantages of the e-MLP method in a problem with complicated wave interactions, MLP5 and e-MLP5 were applied to a normal shock wave/vortex flow interaction problem. The details of the shock wave with a single vortex were as follows: a normal shock wave with a Mach number of 1.29 was propagating into a stationary vortex with a vortex Mach number $M_v = 0.39$ and induced a complex shock/vortex interaction. The initial vortex flow distributions were the same as the isentropic vortex [20,21].

The computational domain ranges were $-20 \leqslant x \leqslant 5$ and $-20 \leqslant y \leqslant 10$ with equal grid spacing. The vortex core was located at $(-5\,-5)$ and the normal shock wave moved toward the vortex from the boundary at x=10. And M-AUSMPW+ and the third order of the Runge–Kutta time integration method were used. Here, the 801×801 grid was used as the baseline grid and the 1601×1601 grid with MLP5 was utilized as the reference grid to show the accuracy of e-MLP5 as compared with MLP5.

The regions classified by the distinguishing process of e-MLP5 with $\varepsilon = 0.001$ are presented in Fig. 19. This figure shows that the normal shock region is determined as a nonlinear discontinuous region, as expected. The majority of the

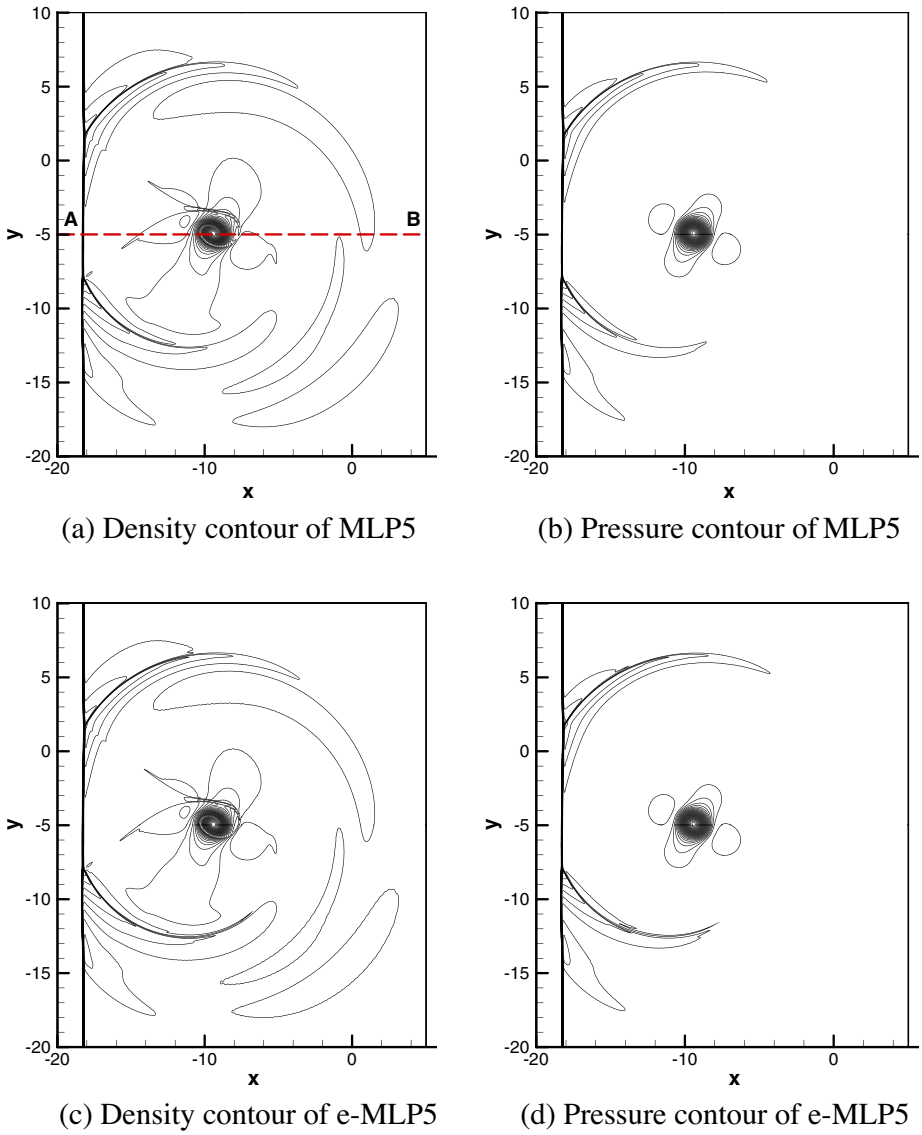

(a) Density contour of MLP5 (b) Pressure contour of MLP5

(c) Density contour of e-MLP5 (d) Pressure contour of e-MLP5

Fig. 20. Density and pressure contours in normal shock wave/vortex interaction flow (801×801 grid).

computational domain is determined as a continuous region; the percentages of the continuous, linear discontinuous and nonlinear discontinuous regions are 98.45%, 0.31% and 1.24%, respectively. Near the core vortex region, several linear discontinuous regions are observed. Those arise because the density distribution changes rapidly at the core region under the current grid set. If the number of grid points is sufficient to represent the region smoothly, then the core region may be selected as a continuous region. Through reduction of the application of TVD criterion and MLP limiter, the overall computational time decreased from 6360 s to 5050 s; hence, the overall computational cost diminished by 21%.

Fig. 20 shows a comparison of density and pressure contours between MLP5 and e-MLP5 after a non-dimensional time of 18. Fig. 20(c) and (d) show that there is no oscillation behavior; e-MLP5 presents nearly the same level of shock stability compared to MLP5. Fig. 21 shows density distributions of MLP5, e-MLP5 and the reference results along the line A-B for a more precise comparison of the solutions. In this figure, e-MLP5 shows a substantial enhancement in the level accuracy compared to MLP5. The results of e-MLP5 with the 801 $\times$ 801 grid are in good agreement with those of the 1601 $\times$ 1601 grid with MLP5.

6.7. Magnetohydrodynamic cloud-shock interaction problem

Generally, MHD equations are associated with complex flow patterns due to the interactions between various MHD waves, such as fast shock waves, slow shock waves, Alfven waves and entropy waves. For such cases, it has been reported

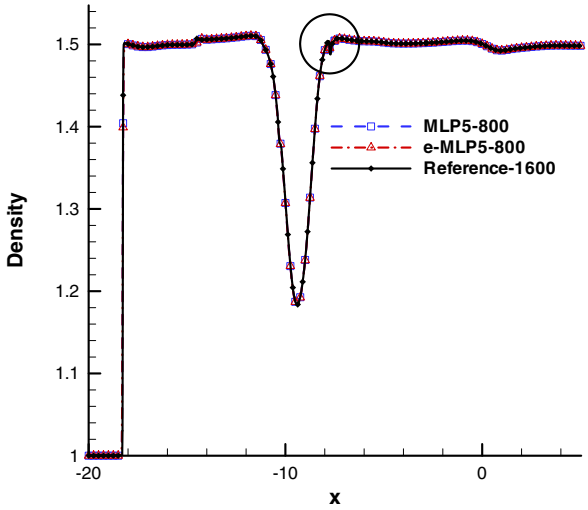

(a) Density distribution along line A-B

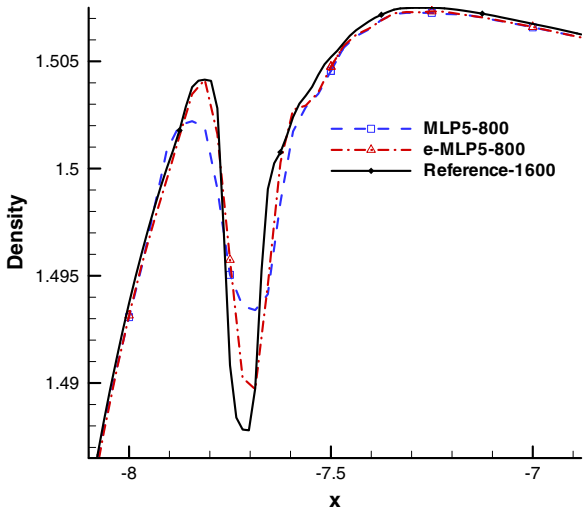

(b) Detailed density distribution at the indicated region

Fig. 21. Comparison of density distributions in normal shock wave/vortex interaction flow.

that the second order TVD van Leer limiter or MC limiter failed to compute a feasible solution due to violent collisions between shocks and clouds [22]. Therefore, in order to assess the robustness of e-MLP, it was applied to a MHD cloud-shock interaction problem that modeled the disruption of a high density cloud by a strong shock wave [22].

The computational domain was $0 \leqslant x, y \leqslant 1$ with uniform 800×800 and 1600×1600grids. The initial condition contained a discontinuity located at $x = 0.6$. The left and right states were expressed by Eq. (29).

$$\begin{aligned} &0 \leqslant x \leqslant 0.6 : (\rho, u, v, w, p, B_x, B_y, B_z) = (3.869, 0, 0, 0, 167.345, 0, 2.183, -2.183), \\ &0.6 \leqslant x \leqslant 1 : (\rho, u, v, w, p, B_x, B_y, B_z) = (1, -11.254, 0, 0, 1, 0, 0.564, 0.564) \end{aligned} \tag{29}$$

with $\gamma = 5/3$.

The discontinuity was a combination of a fast shock wave and a rotational discontinuity in B_z and the rotational discontinuity did not affect the evolution of other flow variables. The circular cloud was located at $x = 0.8$, $y = 0.5$ with a radius 0.15, $\rho = 10$ and $p = 1$. There was a fixed boundary condition at x=1 and other boundaries were zero-gradient boundary conditions [22]. For numerical simulations, M-AUSMPW+ was used for flux evaluation and the third order of the Runge–Kutta method was utilized for time integration with a non-dimensional time of 0.05.

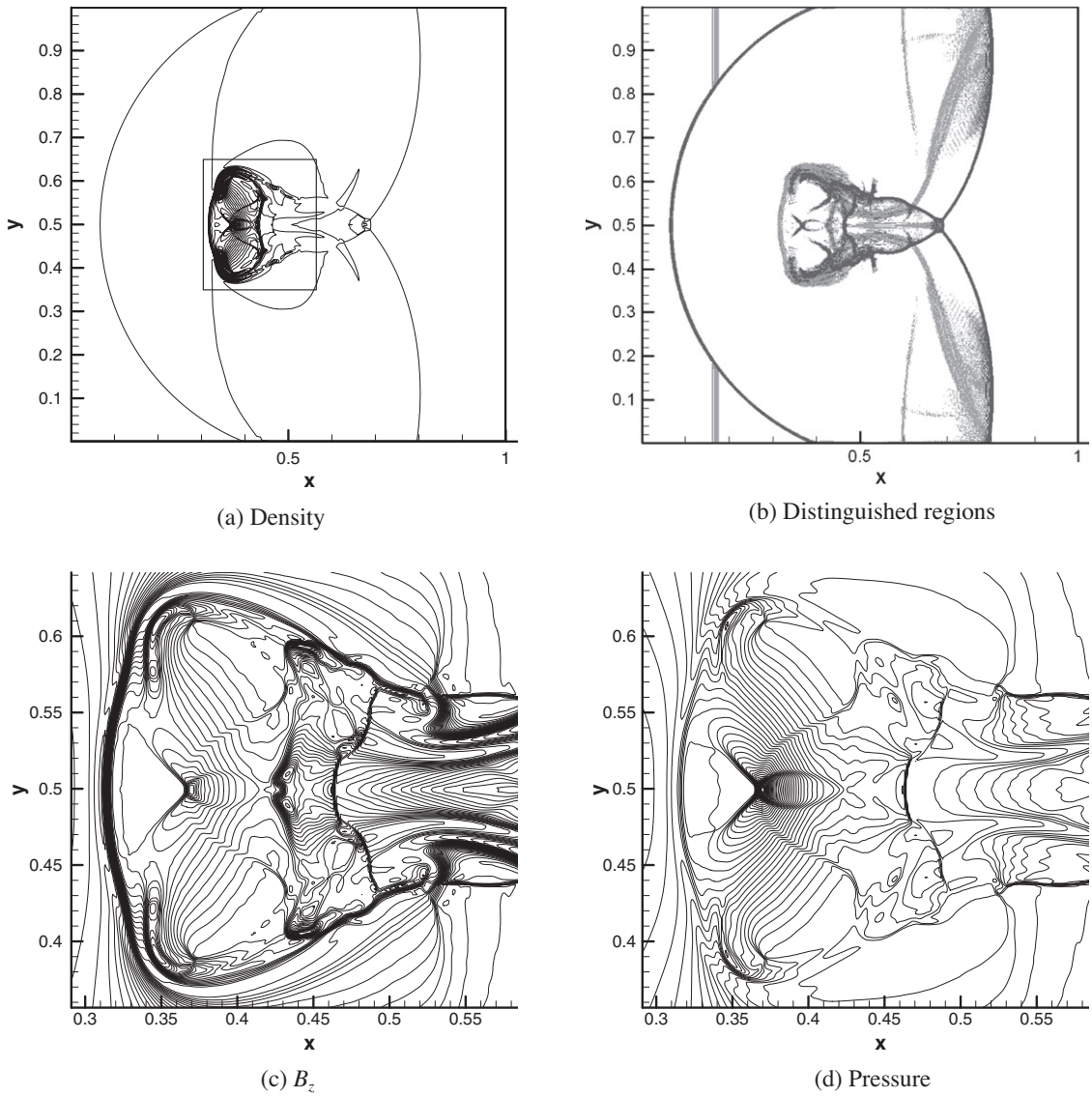

Fig. 22. Density, B_z, pressure contours and distinguished regions in cloud-shock interaction problem. (□: Continuity, ▒: Linear discontinuity, ■: Nonlinear discontinuity).

Density, pressure, B_z contours and the regions classified by e-MLP5 with $\varepsilon = 0.001$ are presented in Fig. 22. Generally, the MHD problem is much more complicated than the Euler problem due to the magnetic field. To sense the shock discontinuous region from the entire domain, Eq. (10) was used in the distinguishing step. After this step, the domain showed a complex mixture of continuous, linear discontinuous and nonlinear discontinuous regions as in Fig. 22(b). Due to the complicated flow pattern of B_z, the discontinuous region was somewhat large. Fig. 22(c) shows the contour of B_z. Even though there is no discontinuity in pressure, the magnetic force makes the complex pattern of nonlinear discontinuity at the wake region. Our distinguishing process mainly followed the nonlinear features of B_z. Concerning efficiency, the majority of the computational domain remained a continuous region; the percentages for each region were 87.9%, 8.2% and 3.9%, respectively. Therefore, the overall computational time decreased from 5970 s to 5050 s, which resulted in the better computational efficiency compared to the result of MLP5. In total, 15% of the overall computational cost was reduced.

Fig. 23 shows a comparison of the density contours of MLP5 and e-MLP5 with the mesh size of 800×800 and 1600×1600. In results of MLP5, wiggles were observed in the enlarged regions of density contour, as shown in Fig. 23(a) and (c), which deteriorated the accuracy of the solution. Most upwind flux schemes including Roe's FDS and AUSM type schemes have developed based on gas dynamics and they have shown good characteristics in calculation of shock discontinuity of gas dynamic flow problems. However in MHD, because of the combination with a magnetic field, it is very hard

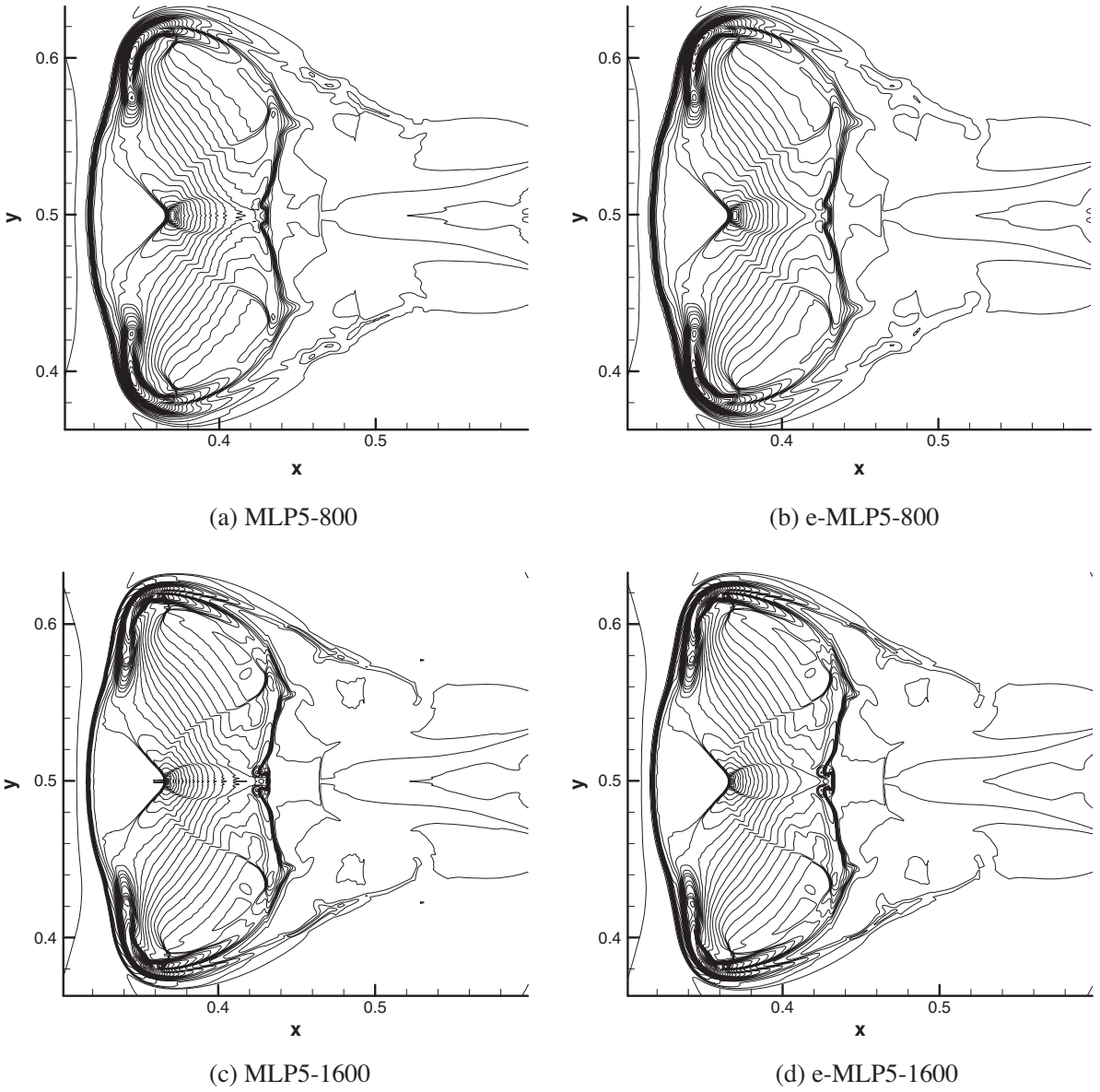

Fig. 23. Comparison of density contours in cloud-shock interaction problem.

to stably calculate a strong shock wave especially with high magnetic Reynolds number. There are no perfect upwind schemes for MHD until now; Different from gas dynamics problems, Roe's FDS and M-AUSMPW+ schemes do not show so perfect features in MHD as in gas dynamics [22,23]. In light of this, to increase the ability of oscillation removal in MHD, it seems to be necessary that additional numerical dissipation be imposed only on a MHD shock region.

The present approach, e-MLP, enhance the ability of oscillation removal in the following way. The crucial advantage of e-MLP is that it can give multi-dimensional information on a shock location to a flux scheme while MLP5 cannot give any information to it because general interpolation schemes including MLP5 are independent of a flux evaluation step. Let us assume that grids are well aligned with a shock discontinuity as shown in Fig. 24 and M-AUSMPW+ is used for flux evaluation. The flux of M-AUSMPW+ are briefly summarized as in Eqs. (30) when the function w is 0 or 1 [13].
when $w = 0$,

$$F_{1/2} = \left(M_L^+ + M_R^-\right) c_{1/2} \mathbf{\Phi}_{L \text{ or } R} + \left(P_L^+ P_L + P_R^- P_L\right), \tag{30a}$$

when $w = 1$,

$$F_{1/2} = \left(M_L^+ c_{1/2} \mathbf{\Phi}_L + M_R^- c_{1/2} \mathbf{\Phi}_R\right) + \left(P_L^+ P_L + P_R^- P_L\right), \tag{30b}$$

where $w = 1 - \min\left(\frac{p_L}{p_R}, \frac{p_r}{p_L}\right)^3$, $\mathbf{\Phi} = (\rho, \rho u, \rho v, \rho H)^T$.

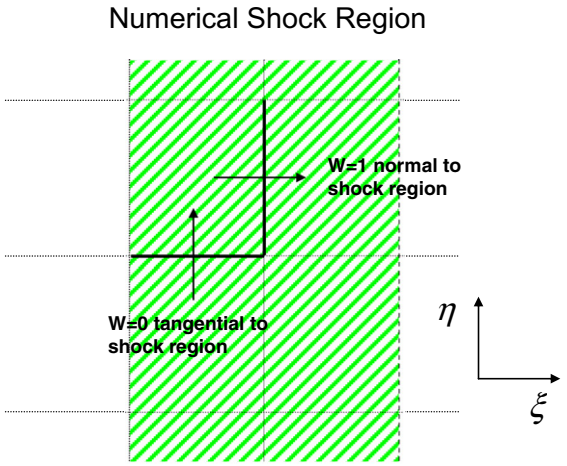

(a) One-dimensional searching (MLP5 with M-AUSMPW+)

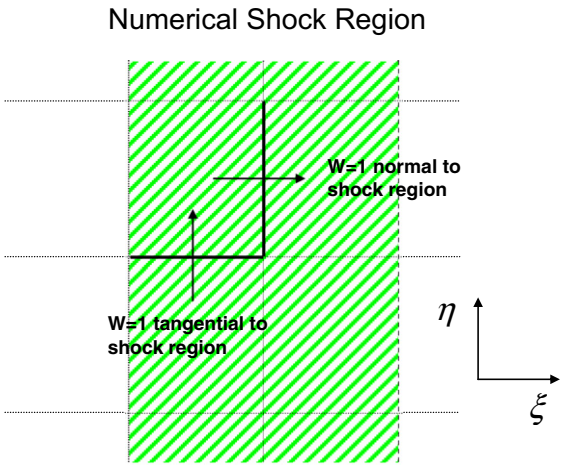

(b) Multi-dimensional searching (e-MLP5 with M-AUSMPW+)

Fig. 24. The difference in the way of shock searching.

M-AUSMPW+ is designed to control the advection property of the AUSM type schemes through the function w and to increase robustness by adding numerical dissipation only to a shock region. If the magnitude of w is small as in Eq. (30a), M-AUSMPW+ have the advection form and the low-dissipation properties like other AUSM type schemes. On the other hand, if the w is nearly 1, it does not maintain the advection form and its form switches into Eq. (30b) that is similar to van Leer scheme, which removes oscillatory behavior in a shock region.

Inside M-AUSMPW+, the existence of numerical shock wave can be recognized only when the normal flux to the shock discontinuity is calculated ($w = 1$). In case of the tangential flux, M-AUSMPW+ cannot notice it and the function w has the value of zero (see Fig. 24(a)). In other words, the combination of MLP5 and M-AUSMPW+ sense the shock location through the one-dimensional searching by the function w of M-AUSMPW+. On the other hand, the present approach of e-MLP finds the shock location independently of a flux evaluation step and then reports the information of shock location to a flux scheme. Therefore, M-AUSMPW+ can notice the existence of shock wave even in the calculation of the tangential flux (see Fig. 24(b)). In the present paper, by help of the multi-dimensional searching of e-MLP, even when the tangential flux along the shock wave was calculated, the value of w was set one, i.e., the numerical dissipation was imposed additionally, which made the calculation more stable.

7. Conclusions

The enhanced Multi-dimensional Limiting Process (e-MLP) is presented for multi-dimensional flows based on MLP. It has a number of typical advantages. First, e-MLP enhances solution accuracy by resolving clipping phenomena at local extrema and excessive damping in linear discontinuous regions; the results of the accuracy enhancement were demonstrated in test cases involving one-dimensional shock/sine wave interaction problem, oblique stationary contact discontinuity, isentropic vortex flow, planar shock/density bubble interaction, and normal shock wave/vortex interaction. Second, e-MLP is robust for shock instability via the multi-dimensional searching of a discontinuity and simultaneous presenting of the information regarding the discontinuity not only to a high order interpolation scheme but also to a flux scheme, which enables the effective addition of numerical dissipation to a nonlinear discontinuous region. Through a high speed flow in a blunt body and a complex MHD cloud-shock interaction problem, e-MLP showed an equal or improved level of robustness compared with MLP. Third, e-MLP improves computational efficiency. In steady state cases including an oblique stationary contact discontinuity and a high speed flow in a blunt body, it generally reduced the overall computational time by nearly 40% compared to MLP via the restricted application of limiting function and the enhancement of convergence. In unsteady cases involving one-dimensional shock/sine wave interaction problem, isentropic vortex flow, planar shock/density bubble interaction, a normal shock wave/vortex interaction and MHD cloud-shock interaction problem, it reduced the overall computational time by approximately 20%. Therefore, in multi-dimensional flow situations with various types of discontinuities, e-MLP is a feasible choice for an oscillation removal scheme due to its level of accuracy, robustness, and efficiency.

Acknowledgements

This work was supported by the second stage of the Brain Korea 21 Project in 2009 for the Mechanical and Aerospace Engineering at Seoul National University. Also, it was supported by NSL (National Space Lab) program through the National Research Foundation of Korea funded by the Ministry of Education, Science and Technology (S10801000121-08A0100-12110).

References

[1] A. Harten, High resolution schemes for hyperbolic conservation laws, J. Comput. Phys. 49 (1983) 357–393.
[2] P.K. Sweby, High resolution schemes using flux limiters for hyperbolic conservation laws, SIAM J. Numer. Anal. 21 (1984) 995–1011.
[3] C. Hirsch, Numerical Computation of Internal and External Flows, vol. 1 & 2, Wiley, UK, 1990.
[4] A. Harten, B. Enquist, S. Osher, S.R. Chakravarthy, Uniformly high order accurate essentially non-oscillatory schemes, III, J. Comput. Phys. 71 (1987) 231–303.
[5] C.W. Shu, TVB uniformly high-order schemes for conservation laws, Math. Comput. 49 (1987) 105–121.
[6] K. Kim, C. Kim, Accurate, efficient and monotonic numerical methods for multi-dimensional compressible flows. Part II: Multi-dimensional Limiting Process, J. Comput. Phys. 208 (2005) 570–615.
[7] S. Yoon, C. Kim, K. Kim, Multi-dimensional limiting process for three-dimensional flow physics analyses, J. Comput. Phys. 227 (2008) 6001–6043.
[8] S. Kim, S. Lee, K. Kim, Wavenumber-extended high-order oscillation control finite volume schemes for multi-dimensional aeroacoustic computations, J. Comput. Phys. 227 (2008) 4089–4122.
[9] M. Brio, C.C. Wu, An upwind differencing scheme for the equations of ideal magnetohydrodynamics, J. Comput. Phys. 75 (1988) 400–422.
[10] P. Janhunen, A positive conservative method for magnetohydrodynamics based on HLL and Roe methods, J. Comput. Phys. 160 (2000) 649–661.
[11] P.L. Roe, Approximate Riemann solvers, parameter vectors and difference schemes, J. Comput. Phys. 43 (1981) 357–372.
[12] K. Kim, C. Kim, O. Rho, Methods for the accurate computations of hypersonic flows, Part I: AUSMPW+ scheme, J. Comput. Phys. 174 (2001) 38–80.
[13] K. Kim, C. Kim, Accurate, efficient and monotonic numerical methods for multi-dimensional compressible flows Part I: Spatial discretization, J. Comput. Phys. 208 (2005) 527–569.
[14] C.W. Shu, S. Osher, Efficient implementation of essentially non-oscillatory shock-capturing schemes, J. Comput. Phys. 77 (1988) 439–471.
[15] C.W. Shu, S. Osher, Efficient implementation of essentially non-oscillatory shock-capturing schemes, II, J. Comput. Phys. 83 (1989) 32–78.
[16] H.C. Yee, N.D. Sandham, M.J. Djomehri, Low-dissipative high-order shock-capturing methods using characteristic-based filters, J. Comput. Phys. 150 (1999) 199–238.
[17] S. Kim, C. Kim, O. Rho, S. Hong, Cures for the shock instability: development of a shock-stable Roe scheme, J. Comput. Phys. 185 (2003) 342–374.

[18] S.K. Saxena, K. Ravi, Some aspects of high-speed blunt body flow computations with Roe scheme, AIAA J. 33 (1995) 1025–1031.
[19] J.M. Picone, J.P. Boris, Vorticity generation by shock propagation through bubbles in a gas, J. Fluid Mech. 189 (1988) 23–51.
[20] J.L. Ellzey, M.R. Henneke, J.M. Picone, E.S. Oran, The interaction of a shock with vortex: shock distortion and the production of acoustic waves, Phys. Fluids 7 (1995) 172–184.
[21] O. Inoue, Y. Hattori, Sound generation by shock–vortex interactions, J. Fluid Mech. 380 (1999) 81–116.
[22] G. Tóth, The $\nabla \cdot B = 0$ constraint in shock-capturing magnetohydrodynamics codes, J. Comput. Phys. 161 (2000) 605–652.
[23] S. Han, J. Lee, K. Kim, Accurate and robust pressure weight advection upstream splitting method for magnetohydrodynamics equations, AIAA J. 47 (2009) 970–981.